# The relationship of dynamical heterogeneity to the Adam-Gibbs and random first-order transition theories of glass formation

Francis W. Starr,[1] Jack F. Douglas,[2] and Srikanth Sastry[3]
[1]*Physics Department, Wesleyan University, Middletown, Connecticut 06459, USA*
[2]*Materials Science and Engineering Division, National Institute of Standards and Technology, Gaithersburg, Maryland 20899, USA*
[3]*TIFR Centre for Interdisciplinary Sciences, Tata Institute of Fundamental Research, 21 Brundavan Colony, Narsingi, Hyderabad 500 075, India and Jawaharlal Nehru Centre for Advanced Scientific Research, Jakkur Campus, Bangalore 560064, India*

(Received 1 October 2012; accepted 15 January 2013; published online 25 February 2013)

We carefully examine common measures of dynamical heterogeneity for a model polymer melt and test how these scales compare with those hypothesized by the Adam and Gibbs (AG) and random first-order transition (RFOT) theories of relaxation in glass-forming liquids. To this end, we first analyze clusters of highly mobile particles, the string-like collective motion of these mobile particles, and clusters of relative low mobility. We show that the time scale of the high-mobility clusters and strings is associated with a diffusive time scale, while the low-mobility particles' time scale relates to a structural relaxation time. The difference of the characteristic times for the high- and low-mobility particles naturally explains the well-known decoupling of diffusion and structural relaxation time scales. Despite the inherent difference of dynamics between high- and low-mobility particles, we find a high degree of similarity in the geometrical structure of these particle clusters. In particular, we show that the fractal dimensions of these clusters are consistent with those of swollen branched polymers or branched polymers with screened excluded-volume interactions, corresponding to lattice animals and percolation clusters, respectively. In contrast, the fractal dimension of the strings crosses over from that of self-avoiding walks for small strings, to simple random walks for longer, more strongly interacting, strings, corresponding to flexible polymers with screened excluded-volume interactions. We examine the appropriateness of identifying the size scales of either mobile particle clusters or strings with the size of cooperatively rearranging regions (CRR) in the AG and RFOT theories. We find that the string size appears to be the most consistent measure of CRR for both the AG and RFOT models. Identifying strings or clusters with the "mosaic" length of the RFOT model relaxes the conventional assumption that the "entropic droplets" are compact. We also confirm the validity of the entropy formulation of the AG theory, constraining the exponent values of the RFOT theory. This constraint, together with the analysis of size scales, enables us to estimate the characteristic exponents of RFOT. © *2013 American Institute of Physics*. [http://dx.doi.org/10.1063/1.4790138]

## I. INTRODUCTION

One of the central mysteries of glass formation is the origin of the dramatic increase of relaxation times approaching the glass transition temperature, $T_g$, which is commonly interpreted as an increase of the effective activation energy.[1,2] Since the low temperature ($T$) activation energy typically exceeds the energy of a chemical bond, it is natural to associate this activation process with the reorganization of multiple atoms or molecules. Indeed, there is general agreement that glass-forming liquids are dynamically heterogeneous, exhibiting a significant fraction of particles with extreme high or low mobility relative to the mean, whose positions are spatially correlated.[3–5]

Even before the phenomenology of dynamical heterogeneity was clearly established, Adam and Gibbs[6] (AG) suggested a molecular picture of this kind in 1965, along with specific predictions for the relation of the configurational entropy $S_{\rm conf}$ to the relaxation dynamics. In particular, they proposed that reorganization in a liquid occurs via hypothetical "cooperatively rearranging regions" (CRR), where the activation energy for relaxation is extensive in the number of atoms or molecules that make up the CRR. The AG model attributes the rapid growth of relaxation time approaching $T_g$ to the progressive growth of the CRR size on cooling. However, the AG theory does not include a microscopic description of the CRR, or a concrete prescription for identifying them. AG further argued that the configurational entropy per CRR is roughly independent of temperature so that the CRR mass is inversely proportional to the configurational entropy of the fluid—a quantity that can be estimated experimentally by the difference of the total and vibrational entropies. Consequently, the entropy formulation of the AG theory postulates that the temperature-dependent activation energy for relaxation is inversely proportional to $S_{\rm conf}$ (the "Adam-Gibbs relationship"). This model has proven to be highly successful to describe the $T$ dependence of relaxation in both experiments[7–9] (where $S_{\rm conf}$ is estimated from specific heat measurements) and computational studies[10–17] (where $S_{\rm conf}$ can be formally evaluated from an energy landscape approach).

 

The random first-order transition (RFOT) theory[18–20] is based upon similar ideas to rationalize the rapid growth of relaxation time on cooling. In particular, the RFOT theory formulates the problem of the relaxation in glass-forming liquids in terms of an "entropic droplet model," or "mosaic" picture, in which the liquid is divided into metastable regions with a characteristic size $\xi$. A consideration of the balance between the surface and bulk free energies of these regions suggests a scaling relation between $\xi$ and $S_{\rm conf}$. The overall barrier for relaxation is also assumed to scale with $\xi$, providing a generalized relationship between $S_{\rm conf}$ and relaxation. Notably, the AG relationship can be recovered by an appropriate limit of RFOT, so that these models are potentially directly linked. As in the case of the AG theory, RFOT theory does not provide a specific molecular definition of the length scale of collective motion. Thus, both the AG and RFOT approaches leave the precise nature of cooperative rearrangements and their relation to dynamical heterogeneity opens to interpretation and quantification.

Computer simulations have been particularly helpful to quantify the nature of dynamical heterogeneity, as the spatial and temporal heterogeneity of glass-forming fluids is difficult to probe directly with experiments. It is now appreciated that atoms or molecules of extreme mobility (or immobility) tend to cluster, and that the most mobile clusters can be further divided into groups of atoms or molecules that move cooperatively in a roughly co-linear, or string-like fashion,[21–27] and this phenomenon has been confirmed experimentally in colloidal particle tracking measurements.[28–31] Consistent with the ideas of the AG and RFOT theories, the sizes of clusters and strings grow on cooling toward $T_g$, but it is not clear if either of these structures are appropriate measures of the size scales envisioned by these theories. Earlier works have considered both the possibilities of using the mobile particle clusters or the strings as the CRR of AG, and each of these studies indicated promising results.[32–35] We should point out that there are other ways to characterize the length scales of heterogeneity. In particular, the use of a four-point correlation function offers an approach rooted in the framework of statistical mechanics that reveals a growing dynamical length scale on cooling.[36–44]

In this work, we systematically dissect cluster and string-like nature of the heterogenous motion in a model glass-forming polymer melt, and then consider what measure or measures of dynamical heterogeneity, if any, may appropriately quantify the size scales envisioned by the AG or RFOT approaches. In doing so, we expand on a general methodology to identify subsets of extreme immobility. Our results span a broad temperature range, from very high $T$, to somewhat below the crossover temperature $T_c$ often associated with mode-coupling theory. We find that, at the characteristic time of maximal clustering, the structures of mobile and immobile clusters exhibit statistical properties that are consistent with the properties of equilibrium branched polymers, which are the same as clusters approaching a percolation transition. When mobile clusters are decomposed into strings, the geometry of short strings are consistent with self-avoiding walks, while larger strings (that appear at low temperature) behave like simple random walks. We find that none of the cluster types that we study forms compact objects when examined at their respective characteristic times. Moreover, the characteristic times of mobile and immobile clusters provide a physically transparent way to understand the decoupling phenomenon, as the mobile cluster time scales have essentially the same temperature dependence as diffusive time scales, while the immobile cluster time scale follows the structural relaxation time. We consider both mobile clusters and strings as possible descriptions of CRR in the AG and RFOT models, and find that the strings – which necessarily incorporate large mobility and cooperativity of displacement – best accord with the quantitative description of the mass or length scales of cooperative clusters described by both these theories.

## II. MODEL AND SIMULATION DETAILS

Our results are primarily based on molecular dynamics simulations of a melt containing 400 chains of "bead-spring" polymers, each chain consisting of 20 monomers.[45] At this length, the chains are unentangled. All monomers interact via a force-shifted Lennard Jones (LJ) potential, truncated at $2.5\sigma$ so that dispersive attractions are included ($\sigma$ is the LJ length parameter). Neighboring monomers along a chain also interact via a finite extensible nonlinear elastic (FENE) spring potential to create covalent bonds. The FENE parameters are $k = 30\epsilon$ and $R_0 = 1.5\sigma$, chosen to create a mismatch in the length scale of bonded and non-bonded interactions, thus frustrating crystallization and making the model a good glass former.[46] All values are reported in reduced LJ units. Standard units for temperature are recovered by multiplying $T$ by $\epsilon/k_B$, where $k_B$ is Boltzmann's constant. Time is given in units of $(m\sigma^2/\epsilon)^{1/2}$. The simulations cover the range of $0.3 < T < 2.5$ at constant density $\rho = 1.0$. For all $T < 1$, we perform five independent simulations to improve statistics. Each simulation consists of an equilibration run followed by data collection; the duration of each run is determined from the $\alpha$ relaxation time (discussed below) to ensure we sample only equilibrium states. Temperature is controlled via the Nose-Hoover algorithm, which is implemented via the reversible reference system propagator algorithm (rRESPA) method using a time step of 0.002 for bond forces with 3 updates for each non-bonded force update.[47]

The dynamics of this model (or the closely related model that excludes LJ attractions) have been extensively studied in previous simulations.[46] To provide basic characterization for subsequent detailed analysis, we first consider the relaxation of the coherent density-density correlation function $F(q, t)$ (Fig. 1(a)). We evaluate $F(q, t)$ at the wave vector $q_0$ corresponding to the first peak of the structure factor where relaxation is slowest (except for the limit $q \to 0$). We define the $\alpha$-relaxation time by $F(q_0, \tau_\alpha) = 0.2$. The $T$-dependence of $\tau_\alpha$ (Fig. 1, inset) is characterized by simple Arrhenius behavior for $T > T_A$; for $T_g < T < T_A$, $\tau_\alpha$ grows significantly faster on cooling, and is well-approximated by the ubiquitous Vogel-Fulcher-Tamman (or Williams-Landau-Ferry) expression:

$$\tau_\alpha = \tau_0 \exp\left[\frac{DT_0}{T - T_0}\right], \tag{1}$$

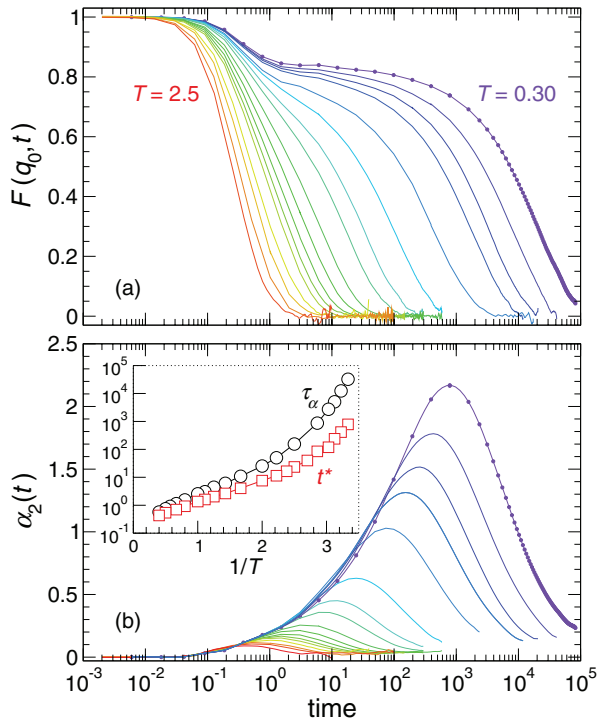


FIG. 1. Characterization of basic dynamical properties of the polymer melt. (a) The coherent density-density correlation function $F(q_0, t)$ for all $T$. The $\alpha$-relaxation time $\tau_\alpha$ is defined by $F(q_0, \tau_\alpha) = 0.2$. Symbols are shown for the lowest $T$ to indicate typical intervals at which data are collected. (b) The non-Gaussian parameter $\alpha_2(t)$ at each $T$ shows a peak due to the correlated motion that occurs roughly on the time scale of $t^*$, defined by the maximum of $\alpha_2(t)$. The inset compares the behavior of $\tau_\alpha$ and $t^*$.

where $T_0$ is an extrapolated divergence temperature that is typically slightly below the laboratory glass transition temperature $T_g$, and $D$ characterizes the curvature (or fragility) of $\tau_\alpha$. From our simulations, the crossover from Arrhenius behavior $T_A \approx 0.8$ and $T_0 = 0.20 \pm 0.01$. For this system and density, the characteristic temperature $T_c$ associated with power-law behavior $\tau \sim (T - T_c)^{-\gamma}$ has been estimated to be $T_c = 0.35$;[48] thus, we probe $T$ significantly below $T_c$. Additionally, we also know that $T_g \approx 1.2\,T_0$ from the simple and widely used convention $\tau_\alpha(T_g) = 100$ s.[34] For a simple polymer (like polystyrene) with $T_g \approx 100\,^\circ$C, the reduced units can be mapped to physical units relevant to real polymer materials, where the size of a chain segments $\sigma$ is typically about 1–2 nm, time is measured in ps, and $\epsilon \approx 1$ kJ/mol.

Since we will examine in detail the spatial heterogeneity of the segmental dynamics, we also evaluate the non-Gaussian parameter $\alpha_2$ as a basic indicator of the time scale and strength of correlated motion (Fig. 1(b)). The peak of $\alpha_2$ defines the time $t^*$, which provides a characteristic time scale of the spatially heterogeneous motion. The amplitude of the peak of $\alpha_2$ also increases, a consequence of the increasing degree of spatial correlations of the motion. Although it is not explicitly documented, it is implicit from many previous works[5,49–52] that $t^*$ grows less rapidly than $\tau_\alpha$ on cooling, as confirmed in the inset of Fig. 1(b). In other words, these characteristic times "decouple." This can be expected since $t^*$ is a diffusive time scale (see Appendix A), and the diffusion coefficient $D$ has long been known to decouple from structural relaxation.[3] AG never envisioned that glass-forming liquids should be characterized by multiple relaxation times; consequently, they did not distinguish between mass diffusion and momentum diffusion (i.e., viscous relaxation), but their language clearly relates to modeling mass diffusion. Fortunately, since these time scales maintain a fractional power-law relation over a large range extending from $T_g$ to $T_A$, the AG (or RFOT) approaches can be equally applied to either mass or momentum diffusion, a point that we expand upon below.

## III. DYNAMICAL CLUSTERS APPROACHING THE GLASS TRANSITION

It is widely appreciated that, below the onset temperature $T_A$, the dynamics become increasingly spatially heterogeneous approaching $T_g$. Regions with either enhanced mobility or diminished mobility form in a spatially correlated manner, and the motions within mobile regions can be further dissected into more elementary groups that move in a string-like, cooperative fashion. In this section, we examine several ways to characterize correlations in mobility and analyze the geometry of these structures.

### A. Mobile and immobile clusters

Since the distribution of particle mobilities varies continuously, the first challenge is how to distinguish mobility subsets. For a variety of systems,[5,51–53] it has been shown that choosing the subset of particles that have moved farther than is expected from the Gaussian approximation at the characteristic time $t^*$ offers a useful metric to identify the highly-mobile particles. Depending on the system, these mobile particles typically account for 5%–7% of the particles below $T_A$. This is also true for the present system, confirmed in our own calculations and in Ref. 52. Accordingly, we follow the choice of Ref. 52 where the same model was examined, and select mobile particles as the 6.5% of particles with the greatest displacement over any chosen interval $t$. This allows us so see the evolution of mobile particle properties over all $t$.

At the other mobility extreme, we identify particles of extreme *immobility*. While a variety of methods to identify low mobility particles have been explored in past literature,[5,54–61] there is considerable variation in the details of these approaches. Moreover, many studies of immobile particles do not condition the selection on mobility, but rather on local packing considerations (e.g., icosahedral packing, Frank-Kasper clusters, a sufficient number of neighbors, etc.). Such attempts are potentially valuable for relating structure to dynamical behavior, but in the present work we wish focus purely on dynamical considerations that should be applicable to characterizing mobility all glass-forming liquids, rather than any particular fluid having its own unique type of local ordering. Consequently, we have developed a criterion for immobile particles based on the tendency for "caged particles" to cluster. We provide a detailed description of the method in Appendix B to avoid breaking the flow of our main results. Broadly speaking, we can identify caged particles for any time $t$ by those particles with displacements smaller than the (weakly $T$-dependent) plateau value observed in the mean-squared displacement. We then find the time at which these caged particles form the largest clusters and evaluate

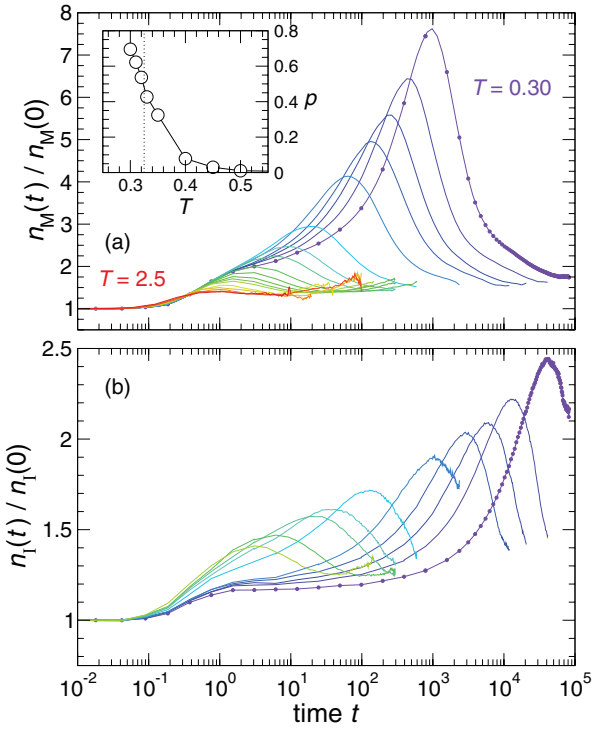


FIG. 2. The dynamical average cluster size for (a) high-mobility particles $\langle n_M(t)\rangle$ and (b) low-mobility particles $\langle n_I(t)\rangle$ at all $T$ studied. The data are normalized by the value at $t = 0$, equivalent the cluster size of the same fraction of particles chosen at random. The definitions of the mobility groups are discussed in the main text. The inset of part (a) shows the percolation probability $p$ of mobile particle clusters as a function of $T$; the dotted vertical line indicates the temperature where $p \approx 0.5$, a standard identifier of the percolation transition in finite-sized systems.[62] For immobile particle clusters, $p < 0.2$ for all $T$, so that percolation is not prevalent.

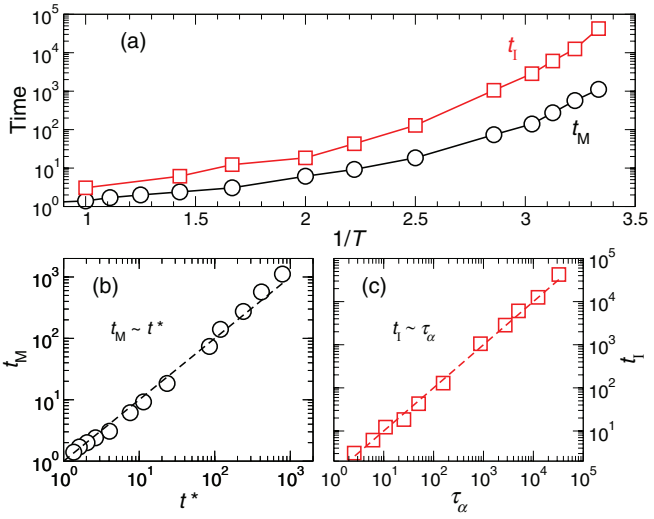


FIG. 3. (a) Characteristic time where the cluster size peaks for mobile (black circles) and immobile (red squares) clusters. Note the similarity to the behaviors of $\tau_\alpha$ and $t^*$, shown in Fig. 1(b). (b) and (c) Parametric plots that show that $t_M \sim t^*$ and $t_I \sim \tau_\alpha$; the dashed lines indicate an equality between these quantities.

what fraction of the system these caged particles constitute. Similar to the approach for mobile-particle clusters, we fix this fraction for all $t$ to track the evolution of the clustering of the immobile particles. Note that the fraction of immobile particles from this method is $T$-dependent, increasing from ≈5 % at the lowest $T$ studied up to 11% at $T_A$. Above $T_A$, the cage size is not well defined.

Having identified the most and least mobile particles at each interval $t$, we examine the average cluster size of the mobile $\langle n_M(t)\rangle$ and immobile $\langle n_I(t)\rangle$ subsets. We plot the cluster sizes (Fig. 2) relative to the cluster size of the same fraction of particles chosen randomly; for immobile particle clusters, this eliminates the trivial $T$-dependence of immobile particle cluster size that arises from $T$-dependence of the fraction of immobile particles (see Appendix B for further discussion). We define a cluster by the group of nearest-neighbor particles that have a separation less than the nearest-neighbor distance, given by the distance of the first minimum $r_{\min} = 1.46$ in the density-density pair correlation function. Figure 2 shows the typical behavior for mobile particle clusters; namely, $\langle n_M(t)\rangle$ peaks at a characteristic time $t_M$ that increases on cooling, and that the peak value $\langle n_M(t_M)\rangle$ also grows on cooling, indicating an increase in the spatial extent of correlations. The immobile particle clusters exhibit the same qualitative trend. Note that we plot the average cluster size, not the *weight*-averaged cluster size; the qualitative behavior of both is same.

There are significant differences between $\langle n_M(t)\rangle$ and $\langle n_I(t)\rangle$ to consider. First, we see that the relative peak size of the mobile particle clusters is larger and increases more rapidly on cooling than that of the least mobile clusters. At the lowest $T$ studied, the mobile particle clusters become so large that the percolation probability $p$, defined as the fraction of configurations with a spanning cluster, approaches unity (inset of Fig. 2(a)). If we define the percolation threshold by $p_c = 0.5$ (as is common in finite systems[62]), the percolation temperature $T_p \approx 0.32$ for mobile particle clusters. Consequently, we likely underestimate the size of mobile particle clusters at the three lowest $T$ studied. For the immobile particles clusters, $p < 0.2$ for all $T$, so that finite-size effects should not be of concern.

The characteristic time scales of these cluster types differ significantly at low $T$. Specifically, the time scale for the peak of the mobile particle clusters $t_M$ is significantly smaller than the peak time $t_I$ of the immobile particle clusters (Fig. 3), similar to the difference in the time scale between $t^*$ and $\tau_\alpha$. Indeed, parametrically plotting these quantities shows that $t_M \sim t^*$ and $t_I \sim \tau_\alpha$ (Figs. 3(b) and 3(c)), and in fact the respective quantities are nearly equal. The similarity between $t_M$ and $t^*$ has been previously noted.[33] The linear scalings can be understood in the context of decoupling phenomena. Specifically, it is widely observed that $\tau_\alpha$ grows more rapidly on cooling than the time scale associated with the diffusion coefficient $D$, giving rise to a breakdown in the Stokes-Einstein relation $D/T \sim \tau_\alpha$—the same decoupling phenomenon previously discussed for $t^*$. Decoupling can be qualitatively understood as a consequence of dynamical heterogeneity, since $D$ will be dominated by the most mobile particles, while relaxation functions (and hence $\tau_\alpha$) will arise from the least mobile particles. Consequently, we anticipate, and indeed observe, decoupling between the $t_I$ and $t_M$ timescale that matches the decoupling between the $t^*$ and $\tau_\alpha$ timescales.

### B. Cluster size distribution and fractal dimension

We next provide a more complete account of the geometrical properties of these clusters. Figure 4 provides a visualization of typical mobile and immobile particle clusters. To quantify the structure of these clusters, we first consider the size distribution $P(n)$ of the clusters at the characteristic times $t_M$ and $t_I$ of the mobile and immobile clusters, respectively. This distribution for mobile particle clusters has been previously examined for a variety of systems, where it is appreciated that $P(n)$ can be described by a power law with an exponential cut-off, namely,

$$P(n) \sim n^{\tau_F} \exp(n/n_0), \tag{2}$$

where $n_0$ is proportional to $\langle n \rangle$. This distribution arises in the description of equilibrium branched polymers and clusters approaching a percolation transition (commonly referred to as "lattice animals"). We shall return to this analogy to help understand our findings. The Fisher exponent $\tau_F$ (using standard notation from percolation theory[62]) should not be confused with a time scale.

Figure 5 shows that both the mobile and immobile particle clusters follow Eq. (2), albeit with different exponents $\tau_F$. For mobile-particle clusters, we find $\tau_F = 1.85 \pm 0.1$. Note that earlier work[52] for this same model indicated $\tau_F \approx 1.6$, but that work was limited to much smaller clusters, and as a consequence was dominated by the behavior at small $n_M$. Our $\tau_F$ estimate is consistent with that for mobile particle clusters in the Kob-Andersen binary LJ liquid ($\tau \approx 1.86$),[5] and slightly larger than that for the Kob-Andersen lattice gas model ($\tau \approx 1.6$). All these $\tau_F$ estimates are smaller than found in percolation theory near the percolation transition in 3D ($\tau_F = 2.18$).[62] These variations suggest that $\tau_F$ may be material dependent. The mass distribution $P(n)$ of the least-mobile particle clusters exhibits similar scaling features to $P(n)$ for the most-mobile clusters, but the exponent $\tau_F$ differs. In particular, $\tau_F \approx 2.2$ is close to that expected for percolation, although assignment of a precise numerical value to $\tau_F$ for the least-mobile clusters is difficult, given the present data.

We can better understand the value of $\tau_F$ by considering the possibility that mobile and immobile particle clusters are analogous to equilibrium branched polymers, which are directly related to percolation clusters. In three dimensions, it is known that $\tau_F$ ranges from 1.5 to about 2.2 for lattice animals[63–65] and percolation clusters,[62,66] respectively, so that $\tau_F$ for branched polymers can be expected to be somewhat variable. This exponent reflects the effect of strong excluded volume interactions between and within these different types of model branched polymers. In mean field theory, which applies above 8 and 6 dimensions for lattice animals and percolation clusters, respectively, where the mean field exponent $\tau_F$ is exactly equal its classical Flory-Stockmayer estimate 5/2. Basically, lattice animals are swollen branched polymers and percolation clusters are branched polymers with screened excluded volume interactions so that these structures are branched polymer analogs of self-avoiding and random walk (more precisely, $\theta$-polymers) polymers describing equilibrium linear polymer chains. In short, our exponent

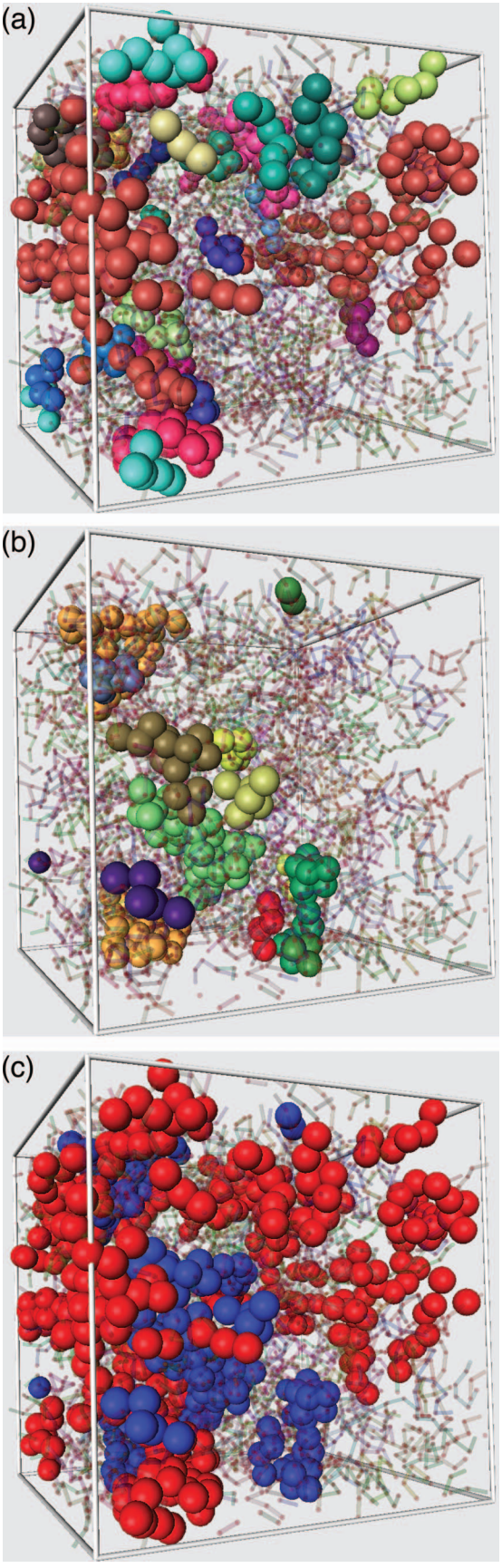


FIG. 4. Typical examples of (a) the most mobile and (b) least mobile clusters. Different clusters are shown in different colors, and the segments of all chains are shown translucent. (c) The same mobile clusters (all colored red) and immobile clusters (all colored blue) to facilitate comparing their relative spatial distribution.

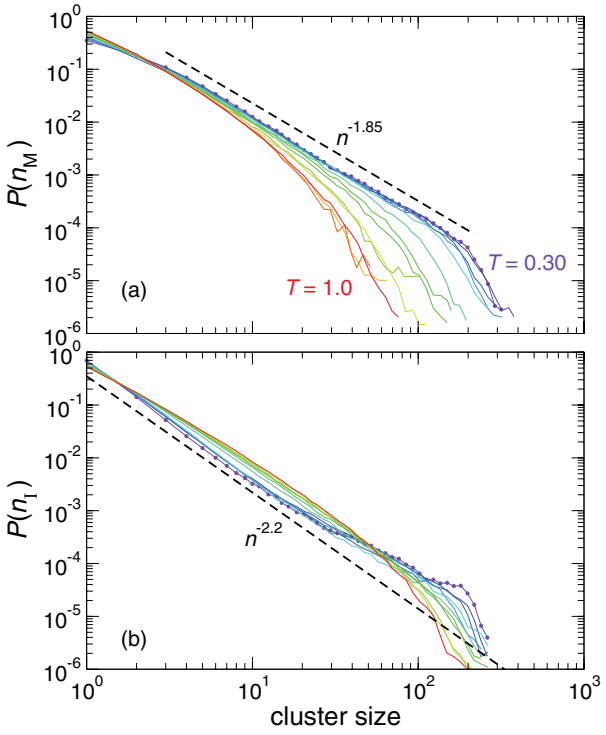


FIG. 5. The distribution of particle cluster sizes $P(n)$ for (a) mobile and (b) immobile particle clusters. The distribution can be described by a power-law with an exponential cut-off, like clusters nearing the percolation transition. The dashed lines indicate a characteristic power-law. Different colors represent different $T$, as in previous figures.

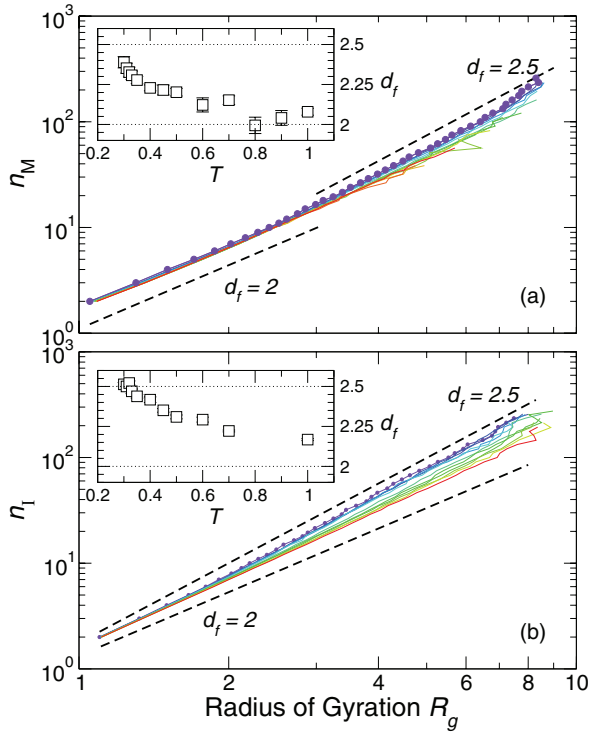


FIG. 6. Scaling of cluster mass $n$ with the radius of gyration $R_g$ to define the fractal dimension $d_f$ of (a) mobile and (b) immobile particle clusters. The solid lines represent the simulation results, and different colors indicate different $T$, as in previous figures. Small circular symbols are shown for the lowest $T$, to indicate the density of data. The bold dashed lines are a guide to the eye, and provide approximate bounds on $d_f$. This is more clearly seen in the insets, which show the $T$ dependence of $d_f$. The dashed lines of the insets indicate the limiting behaviors discussed in the text.

estimates for $\tau_F$ are consistent with the expected exponent range for branched polymers.

To further characterize the geometrical structure of these clusters at their characteristic peak times, we examine the fractal dimension $d_f$ of the clusters defined by the scaling of cluster size

$$n \sim R_g^{d_f}, \tag{3}$$

where

$$R_g^2 = \frac{1}{2N}\sum_{i,j}(r_i - r_j)^2 \tag{4}$$

is the radius of gyration, and $i$ and $j$ denote particles indices within a given clusters. Earlier work has suggested that $d_f \approx 2$ for mobile particle clusters,[67,68] which corresponds to the value for lattice animals in 3D—that is, percolation clusters below the percolation threshold $p_c$. For mobile-particle clusters, we indeed find that smaller clusters have $d_f \approx 2$ (Fig. 6). However, for larger clusters, which only occur for lower $T$, it appears the scaling crosses over to a larger $d_f \approx 2.5$. Since the appearance of these large clusters occurs only at low $T$, extracting the best fit result for $d_f$ at each $T$ results in the effective $d_f$ growing from roughly 2 to near 2.5 on cooling (insets of Fig. 6). For immobile clusters, the scaling of mass on $R_g$ for small and large clusters does not noticeable change with size. As in the case of mobile clusters, $d_f$ grows from 2 to near 2.5 on cooling. Thus, there is significant similarity in the geometrical structure of the mobile and immobile particles clusters. However, the precise values of $d_f$ should be taken with caution, since the range of the data covers less than a complete decade in $R_g$.

We can understand the changing value of $d_f$ by again considering the analogy to equilibrium branched polymers and lattice animals. Specifically, lattice animals are self-avoiding branched polymers with strong excluded volume interactions, and have a fractal dimension $d_f = 2$ in three dimensions.[62,69] The mobile and immobile particle clusters conform to this scaling at relatively high $T$, where they are sparse and not strongly interacting with each other. Like the mass distribution exponent $\tau_F$, the fractal dimension $d_f$ of branched polymers is also sensitive to excluded volume interactions. Branched polymers with screened, excluded volume interactions behave like percolation clusters, and have a fractal dimension $d_f \approx 2.5$ in 3D.[62] Thus, if we consider our clusters to be analogues of branched polymers, the increase of $d_f$ upon cooling can be interpreted as the result of screening of their excluded volume interactions. This situation is natural since, as the clusters grow upon cooling, the concentration describing the onset of their mutual interaction will decrease. We note that this crossover in exponent values has been anticipated for the branched polymer structures associated with Coniglio-Klein clusters in the Ising model.[70]

The crossover behavior we observe for the exponent $d_f$ with temperature is not apparent in the size-scaling exponent $\tau_F$. This might be understood from the fact that, in percolation, $\tau_F$ is far less sensitive than $d_f$ to changes in cluster

structure or dimensionality.[62,71] Given that the range of data used to determine $\tau_F$ and $d_f$ is rather modest, further study to determine whether these clusters can be exactly identified with branched equilibrium polymers is merited. Additionally, examination of the anisotropy of clusters will be valuable to improve the comparison to branched polymers, since cluster shape is often a more discriminating metric of the cluster type than the size distribution or fractal dimension.[72]

### C. String-like cooperative motion

Mobile-particle clusters can be further decomposed into subsets of string-like groups of cooperatively moving particles. We now consider the properties of these "strings," following an analysis parallel to that just discussed for the clusters. To identify string formed by mobile particles, we follow the procedures originally developed in Ref. 21. Specifically, using the same mobile particles that we use to identify clusters, we consider two mobile monomers $i$ and $j$ to be in the same string if, over an interval $t$, one monomer has replaced the other within a radius $\delta$. Following Ref. 22, which examined the same polymer model, we choose $\delta = 0.55$, although the results are not strongly sensitive to this choice for reasonable values of $\delta$. Since we study a polymeric system, it is worth noting that the string-like collective motion is not strongly correlated with chain connectivity,[22] so it should not be confused with reptation-like motion.

For reference, we first show the average length (number of monomers) of a string $L(t)$ for all $T$ studied (Fig. 7). As expected, $L(t)$ has a peak at a characteristic time which we label $t_L$, and the time scale and amplitude of this peak grow on cooling, indicating increased cooperative motion nearing $T_g$. Since the strings are subsets of the mobile particle clusters, the peak value of $L$ is significantly smaller than that of the mobile particle clusters. As a consequence, the percolation probability of the strings, even at the lowest $T$ simulated, is negligible.

The characteristic time $t_L$ of the strings (Fig. 8) is similar to $t_M$ for the mobile particle clusters, but is slightly larger, consistent with Ref. 33. Moreover, like $t_M$, $t_L$ scales linearly

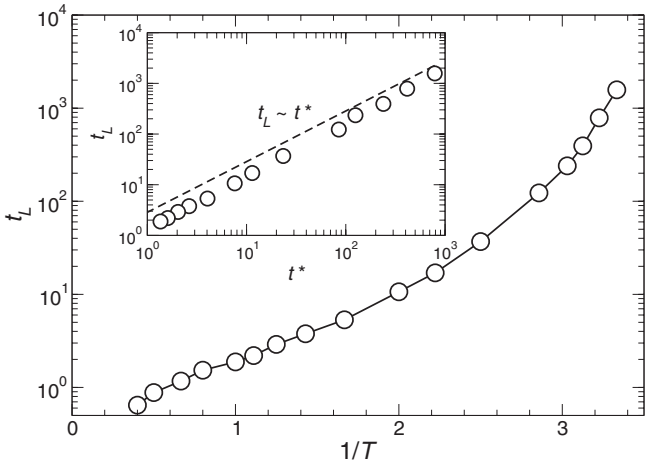


FIG. 8. The characteristic time $t_L$ of the peak string length. The inset shows that, like the characteristic time of mobile particle clusters, $t_L$ scales nearly linearly with $t^*$.

with $t^*$ (Fig. 8 (inset)). Since $t^*$ scales linearly with the characteristic diffusion time (Appendix A), this helps to clarify that the mobile particle time scales captured by the clusters and strings relate to a diffusive relaxation time, rather than the $\alpha$-relaxation time. This time scale is naturally shorter than $\tau_\alpha$ as a consequence of the breakdown of the Stokes-Einstein relation.

To complete the characterization of the strings, we examine the distribution of string lengths $P(L)$ and their fractal dimension at the characteristic time $t_L$. As expected from earlier works,[21,22] Fig. 9 shows that $P(L)$ follows an exponential distribution that is characteristic of linear equilibrium polymers.[73] To estimate the fractal dimension $d_f$, we examine the scaling between $L$ and $R_g$ in Fig. 10. For short strings, we find that $d_f \approx 5/3$, consistent with a self-avoiding walk in 3D. For longer strings, the scaling relation approaches $d_f = 2$, the fractal dimension of simple random walks or self-avoiding walks with screened, excluded volume interactions.[74] This screening effect has been seen in simulations of dynamically associating linear chain polymers.[75] Since longer strings are

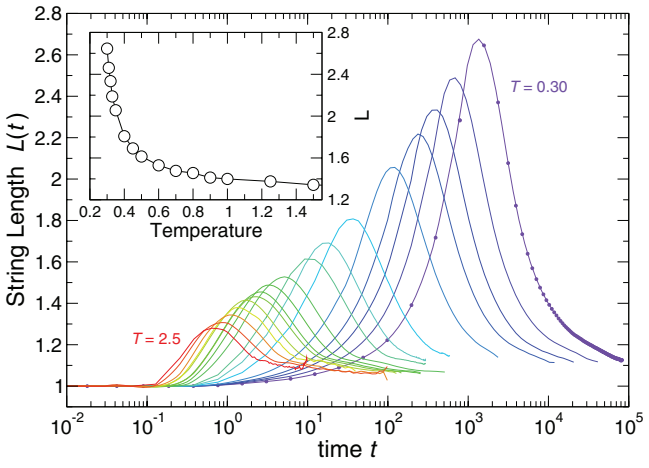


FIG. 7. The dynamical string length $L(t)$ for all $T$ studied. The inset shows the $T$ dependence of the characteristic peak value, simply denoted as $L$.

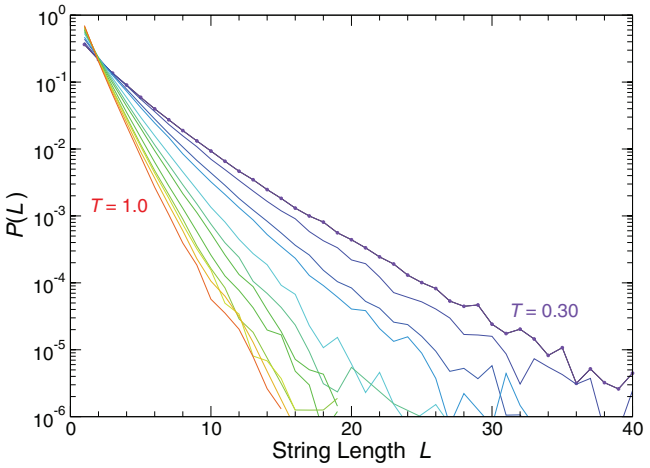


FIG. 9. The distribution of string lengths $P(L)$ follows an exponential law that can be anticipated by analogy with equilibrium polymerization.[73]

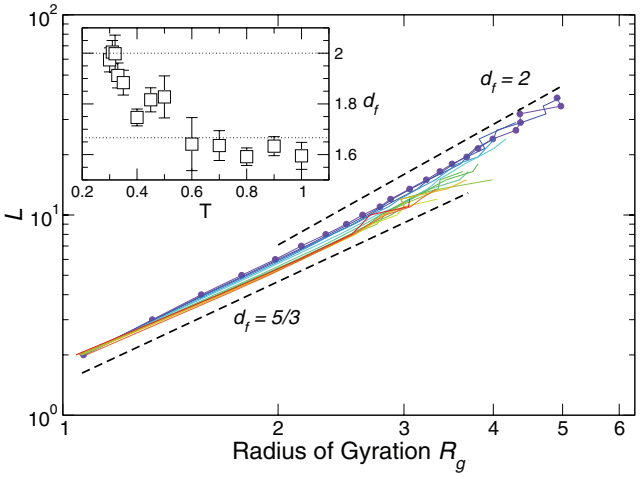


FIG. 10. The scaling $L \sim R_g^{d_f}$ to determine the fractal dimension $d_f$ of strings. The solid lines represent the simulation results, and different colors indicate different $T$, as in previous figures. Small circular symbols are shown for the lowest $T$, to indicate the density of data. The bold dashed lines are a guide to the eye, and provide approximate bounds on $d_f$. This is more clearly seen in the insets, which show the $T$ dependence of $d_f$. The dashed lines of the inset indicate expected limiting behaviors. Specifically, there appears to be a modest change in $d_f$ from ≈5/3 for short strings (the approximate value for a self-avoiding walk in 3D) to ≈2 (a simple random walk, also characteristic of many branched polymers). Accordingly, a typical string at low $T$ is less extended, just as in polymer chains in dilute versus concentrated solutions.

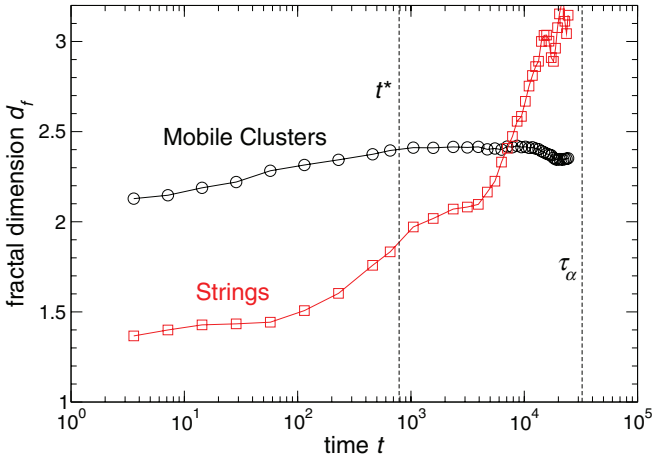


FIG. 11. The temporal evolution of fractal dimension $d_f$ of mobile clusters and strings at the lowest $T = 0.30$. The mobile-particle cluster structure is relatively insensitive to $t$, but the string geometry differs dramatically between $t^*$ and $\tau_\alpha$.

prevalent only at low $T$, the effective $d_f$ from fitting the entire range is $T$-dependent, growing from 5/3 to 2 on cooling (inset of Fig. 10), reflecting an increased screening of excluded volume interactions upon cooling as in the branched dynamic clusters. Hence, the strings appear to become somewhat more irregular in shape on cooling. It has been argued that cooperative motions should become fully compact (i.e., $d_f \to 3$) at low $T$,[76] but we see no indication of such a collapse for any of the cluster types we have examined. As for our data for mobile and immobile particle clusters, the precise values of $d_f$ should be taken with caution, since the range of the data covers less than a complete decade in $R_g$.

The time scale at which one examines cooperativity can be expected to be important in the consideration of the cluster geometry. Thus, we next consider the fact that the geometrical structure of mobile clusters and strings depends on the time scale on which one examines these objects. Our previous analysis focused on $d_f$ at the characteristic peak time of mobile particle clustering and string size, which is close to $t^*$, a time that is significantly smaller (at low $T$) than $\tau_\alpha$. Figure 11 shows the temporal evolution of $d_f$ for the lowest $T$ studied. While $d_f$ for mobile particle clusters is weakly dependent on time, $d_f$ for the strings is indeed strongly dependent on the time scale considered. In fact, on time scales approaching the structural relaxation time, the strings appear compact ($d_f \approx 3$), which may explain contradictory claims that cooperative motions should form compact regions at low $T$.[76] On this long time scale, the strings are quite small. This result emphasizes the fact that it is critical to examine the cooperativity of motion on the appropriate time scale, and thus quantification of these scales is necessary.

## IV. DYNAMICAL SCALES AND RELAXATION

A central challenge in describing glass formation is the origin of the rapidly increasing relaxation time approaching $T_g$. This is the defining characteristic of fragile glass-forming fluids. If one makes a natural assumption that relaxation is an activated process, transition state theory[77–79] indicates a general Arrhenius temperature dependence

$$\tau = \tau_0 \exp[\Delta F/T], \tag{5}$$

that is often observed in condensed phase relaxation process and in the rates of chemical reactions. At high $T$, $\Delta F(T) \equiv \Delta F_A$, a constant, giving the widely known Arrhenius form. At lower $T$, this relation defines a generalized $T$-dependent activation free energy:

$$\Delta F(T) = T \ln \tau/\tau_0, \tag{6}$$

which we show for our data in Fig. 12. This provides a simple parametric description of the problem at hand: how can we understand an activation barrier the grows on cooling to a value that is several times larger than its high-$T$ limit? Approaching $T_g$, this growth typically reaches 4–8 times the high-$T$ limiting value $\Delta F_A$, and the exponential nature of activation leads to extremely large changes in relaxation. The key element to explain the increase of $\Delta F(T)$ is to recognize that such values cannot be readily reconciled on the basis of single particle motion. Both the AG and RFOT approaches are built upon the notion that many particles are involved in relaxation, and the scale grows on cooling toward $T_g$. Accordingly, the change of $\Delta F(T)$ constrains any attempts to explain the change in relaxation time of glass-forming liquids in terms of a growing dynamical size scale. Thus, as a simple starting point, we consider the relative growth of $\Delta F$ with those of the cluster and string sizes in the inset of Fig. 12. We also make the mathematically trivial, but conceptually important point, that the existence of a fractional power law relation between $\tau$ and $t^*$ (fractional Stokes-Einstein relation) implies that the reduced activation energy applies to *both* relaxation times, and indeed all transport properties obeying such a power scaling

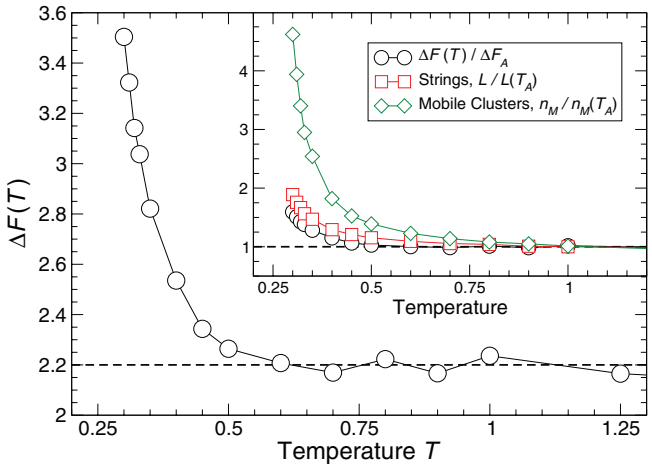


FIG. 12. Temperature dependence of the activation free energy $\Delta F(T)$, evaluated from the relaxation time according to Eq. (6). The dashed line indicates the high $T$ asymptotic value $\Delta F_A = 2.2$. The inset shows values of $\Delta F$, string mass $L$, and mobile cluster mass $n_M$ normalized by their values at $T_A$ to facilitate comparison of the growth of these quantities on cooling.

relationship. This explains why the AG model for diffusive relaxation can be equally well applied to structural relaxation.

### A. Summary of the AG and RFOT predictions

The seminal work of Adam and Gibbs helped to establish a picture of dynamics nearing $T_g$ where motion is dominated by "cooperatively rearranging regions," thereby introducing the importance of a dynamical size scale. Both the AG and RFOT approaches build on the activation picture for dynamics. For most fluids, the high $T$ (i.e., $T > T_A$) dependence of relaxation is given by Eq. (5), where $\Delta F = \Delta F_A$. AG associated this high $T$ activation barrier with uncorrelated, single-particle motion. On cooling toward $T_g$, AG argued that motion becomes dominated by CRR, and that the barrier $\Delta F$ is extensive in the number $z$ of rearranging monomers in a CRR, so that

$$\tau \sim \exp[z\Delta F_A/T]. \tag{7}$$

AG further argue that the fluid can be decomposed into $N/z$ such as CRR, each of which has a configurational entropy $s_{\rm conf}$, so that the total

$$S_{\rm conf} = \frac{N}{z} s_{\rm conf}. \tag{8}$$

Consequently, the relaxation can be directly relating $S_{\rm conf}$ via

$$\tau \sim \exp[A/(TS_{\rm conf})], \tag{9}$$

where the free energy $A$ subsumes previous constants. This configurational entropy picture has proved highly successful in capturing the $T$ dependence of many supercooled fluids.[7–17] Unfortunately the CRR and $S_{\rm conf}$ are not explicitly defined by AG. Fortunately, numerous works have shown that a potential energy landscape-based definition of $S_{\rm conf}$ appears robust;[10–17] other studies have shown that $z$ might be defined in terms of string or mobile cluster size[32–35]—a point we will examine in the context of both AG and RFOT.

The similar RFOT description is built around a scaling description of the problem.[18–20] RFOT theory proposes a "mosaic" picture, in which the liquid is divided into metastable regions with a characteristic size $\xi$ (the "mosaic" length)—conceptually like the CRR idea of AG. RFOT assumes the free barrier for reorganization has a general scaling with size, so that

$$\Delta F \sim \xi^{\psi}. \tag{10}$$

Accordingly, the implication is that $\tau$ scales as

$$\tau \sim \exp[\xi^{\psi}/T]. \tag{11}$$

The free energy of this "droplet" is a balance between the entropic contribution from the degeneracy of states $TS_c\xi^d$ (for a compact droplet in dimension $d$) and surface free energy, which should scale as $\Upsilon(T)\xi^{\theta}$, where $\Upsilon$ is a generalized surface tension of the entropic droplet, and the surface scaling exponent $\theta \leq d-1$. If the entropic droplet is not compact, such as is the case for our clusters and strings, we can generalize this argument simply by replacing $d$ with $d_f$, as in the application of the droplet models to critical phenomena. The ordinary surface tension of many fluids is often found to grow approximately linearly on cooling, and Cammarota *et al.*[80] argue that $\Upsilon$ of RFOT should grow at least linearly on cooling. Thus, assuming $\Upsilon(T) \sim T$ and balancing the surface and volume effects yields a scaling between $\xi$ and configurational entropy,

$$\xi \sim 1/S_{\rm conf}^{1/(d_f-\theta)}. \tag{12}$$

Combining Eqs. (11) and (12) yields the generalized AG-like relation between relaxation and entropy,

$$\tau \sim \exp[A/(TS_{\rm conf})^{\psi/(d_f-\theta)}]. \tag{13}$$

We note that the concept of surface tension here is formally unclear, since there are no explicitly co-existing phases. However, subtle differences in the local packing of highly mobile and immobile particles certainly contributes an energy gradient near the interface of these regions. Similarly, Refs. 81 and 82 found that mobile-particle clusters found in a melting crystal can be identified with the nucleation of a fluid phase, so that the notion of a surface tension proper for mobile regions has a well defined meaning in this context. Further study in glass-forming liquids may illuminate the notion of the mobile particle clusters having a surface tension. Additionally, a more general scaling of $\Upsilon$ than simple proportionality to $T$ would lead to a slightly different scaling relation between $\xi$ and $S_{\rm conf}$.

The values of the exponents $\psi$ and $\theta$ are not fixed in the theory, but on general physical grounds the exponents should obey the inequality $\theta \leq \psi \leq d-1$.[20,83] The well-established entropy form of AG is recovered from RFOT provided that $\psi = (d_f - \theta)$, leaving only one free exponent. The original presentation of RFOT by Kirkpatrick, Thirumalai, and Wolynes[18] presumes $d_f = d$ (compact droplets), and argues that $\theta = d/2$ and $\psi = \theta$, satisfying the AG entropy form and exponent inequality. More recently, the exponents have been examined in a number of computational and experimental analyses;[42,80,84] these studies are inconclusive regarding a universal value, but generally report values $\psi \approx 0.7$–1 and

$\theta \approx 2$–2.3. These values are troubling, since, based on the exponent inequality, we expect the surface scaling exponent $\theta \leq 2$ (for $d = 3$), and further that $\theta$ should be larger than $\psi$.

Both the AG and RFOT methods offer a way to relate the size or length scale of motion with relaxation times, but do not directly specify how this size scale should be measured. Hence, we now consider if the heterogeneity scales defined by mobile clusters or strings might be appropriate for use within these theoretical descriptions. However, we note that, while many recent studies indeed focus on the size scales of heterogenous motion in this context, there are reasons to be cautious, and to consider other possible length scales.[42,85]

### B. Testing the Adam and Gibbs approach

Although the relation between configurational entropy and relaxation (Eq. (9)) proposed by AG is not their starting point, this is the most commonly tested and most broadly supported prediction of the theory. Hence we first wish to test whether this relation is also valid in our system. Evaluation of $S_{\rm conf}$ is a rather cumbersome process, and so we describe the process fully in Appendix C. Figure 13 verifies the validity of Eq. (9). The inset of Fig. 13 shows that extrapolating a simple polynomial fit of $S_{\rm conf}$ to low $T$ yields "Kauzmann" temperature $T_K = 0.20$ where $S_{\rm conf} \to 0$. This is exactly the same value $T_0$ obtained from independently fitting $\tau$ by the VFT function. Hence, the vanishing of $S_{\rm conf}$ coincides with the independently extrapolated divergence of relaxation time, a comforting consistency check. We note that $S_{\rm conf}$ is a relatively small contribution to the overall fluid entropy in comparison to the vibrational entropy of our polymer glass-forming liquid. This fact makes the experimental estimation of the difference between the total and vibrational contributions to the entropy particularly uncertain in polymer fluids, since there is no reliable means of estimating the vibrational entropy to high accuracy.

We now continue to examine the proposal laid out by AG by considering the relation of $\tau$ to a heterogeneity scale. As described above, the foundation of AG is that the activation energy for relaxation is extensive in the mass $z$ of the CRR (Eq. (7)). Since the CRR are not defined by AG, previous works have considered whether the string mass $L$[33,34] or the mobile particle cluster mass $n_M$[33,52] might be appropriate measures. For water, it was shown that $n_M$ has the desired behavior, but over a relatively limited range of $\tau$;[32] for a simple spherically symmetric model, both $L$ and $n_{\rm mobile}$ show the desired relation to $z$, but over an even more limited range.[33] More recently, motivated by description of AG that CRR are the most basic units of reorganization, Refs. 34 and 35 found $L$ is an appropriate measure of $z$, but did not consider cluster size $n_M$. Unfortunately, none of these works could definitively exclude other measures for $z$. It has also been appreciated that other length scales associated with heterogeneity, such as from a four-point density correlation function, would be too large at $T_g$ to be consistent with $z$.[43] We shall return to this point in the conclusion.

Here, we check the plausibility of both cluster and string size as a measure of $z$ over a substantially broader range of $\tau$ than previous works to provide improved clarity. We thus consider substituting for $z$ the peak string size $L/L(T_A)$ or the peak mobile particle cluster size $n_M/n_M(T_A)$, where we normalize by the value at $T_A$ so that $z$ has the expected value near unity for $T \geq T_A$. Figure 14 shows that, for $T \lesssim T_A$ $\log \tau$ is linear if we use $L$ as a proxy for $z$, but not using $n_M$. The deviation from cluster size is a consequence of the fact that the mobile particle cluster size grows noticeably more rapidly than the effective activation free energy, a fact already appreciated in the inset of Fig. 12. If AG is assumed correct at high $T$, such an exponential relation should continue into the $T > T_A$ range, where $z$ should be near unity, or at least reach its asymptotic value. In such a case, the value of $\Delta F$ from the low $T$ fit using Eq. (7) should be comparable to the high $T$ estimate of $\Delta F_A$ from an Arrhenius fit. Using $z = L/L(T_A)$, we estimate $\Delta F = 1.8$, somewhat smaller that the value estimated from the Arrhenius fit, $\Delta F_A = 2.2$. One interpretation of this discrepancy is that using $L(T_A)$ as the normalizing factor is

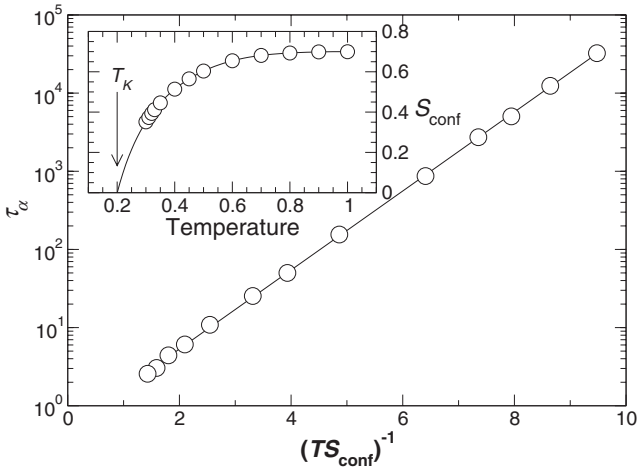


FIG. 13. Confirmation that the entropy representation of the AG theory (Eq. (9)) is valid for the present system. The inset shows the $T$ dependence of $S_{\rm conf}$ and the extrapolating vanishing temperature $T_K$, which is consistent with $T_0$ of the VFT fit (Eq. (1)) to $\tau$.

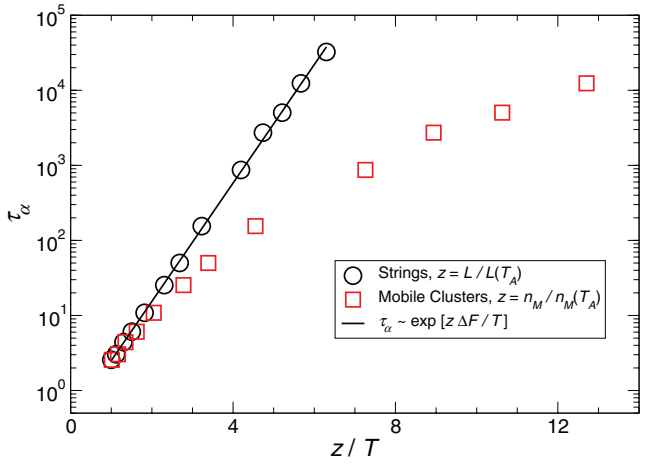


FIG. 14. Testing the mobile particles cluster and string sizes for consistency with the AG prediction that the activation energy is linear in the size $z$ of CRR. The cluster size $n_M$ grows too rapidly on cooling to fit with the AG picture, the string size $L$ appears consistent. See also Fig. 12 for a direct comparison of $L$ and $n_M$ to the relative change in $\Delta F$ with no free parameters in the comparison.

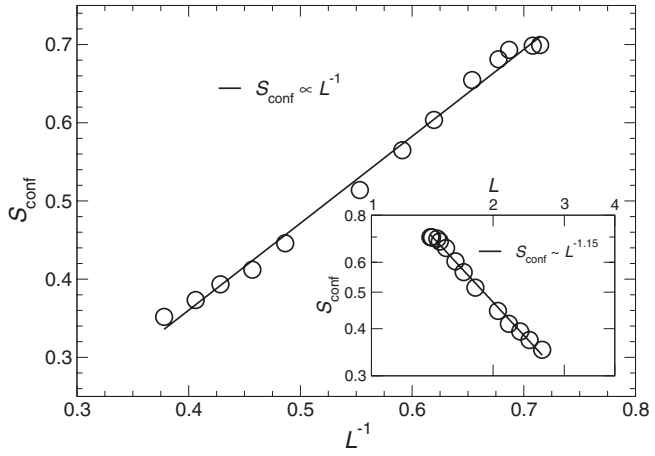


FIG. 15. Testing $S_{conf} \propto 1/L$. The inset checks for the best power-law relation, which yields an exponent slightly larger than one.

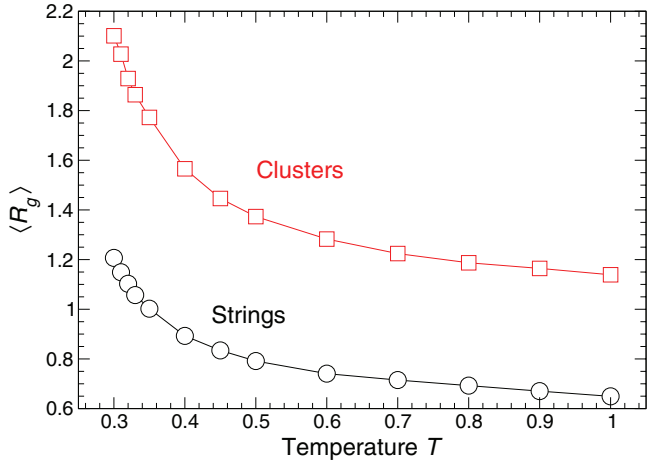


FIG. 16. The mean radius of gyration $\langle R_g \rangle$ for the strings and mobile particle clusters. This defines a characteristic length that we can test within the RFOT framework.

not entirely correct, and a somewhat smaller value would be more appropriate.

Given the apparent success of the string mass $L$ to describe $\tau$ and the broadly reported validity of the entropy formulation of AG, we test for consistency between these representations by checking the expected relation $S_{conf} \propto 1/z$ (Fig. 15). The data support the linearity of the relationship, although there are some systematic deviations at both the lowest and highest $T$. This suggests that, while $L$ captures the generally expected behavior of the CRR, a more detailed refinement of the determination of $L$ may provide a more accurate description of CRR.

The string length $L$ appears to be the most quantitatively valid choice for the CRR, and is also consistent with the qualitative philosophy of AG. Specifically, recall that AG envision the CRR are dominated by the *smallest* group of cooperatively moving monomers. The physical motivation for this is that probability of such a group will diminish exponentially with the size, so that the smallest possible group that allows for rearrangement will dominate the relaxation. The strings are both the smallest such unit, and also the only candidate in which all particles move in a cooperative fashion. While the particles of mobile particles clusters are obviously spatially correlated, there is no *a priori* cooperativity in their displacements. The strings are precisely the manifestation of mobile particle cooperativity. However, we should be careful to point out that, while the qualitative language of AG is appealing, in the end the quantitative predictability is the most important measure. We shall next explore which measure best quantitatively fits with the formulation of the RFOT theory.

### C. Testing the RFOT approach

As discussed in Sec. IV B, the validity of the entropy formulation of AG dictates that $\psi = (d_f - \theta)$. Hence there is only one free exponent in the RFOT formulation. We shall consider two approaches to determine these exponents, which provides an internal consistency check.

A simple, but significant, difference between AG and RFOT is that RFOT refers to a length scale of cooperative motion, rather than the extent or particle mass of collective motion. Consequently, to test whether any of the clusters or strings might be appropriate, we need to consider a length scale that defines the size of mobile clusters or strings. The natural length scale for these objects is the radius of gyration $R_g$ at their respective characteristic times, which we show in Fig. 16. Hence we can directly evaluate the exponent $\psi$ from the scaling of $\tau$ with $\langle R_g \rangle$ (Eq. (11)) for the strings and clusters.

Figure 17 shows the scaling of $\tau$ with $\langle R_g \rangle$ for the strings and clusters, from which we obtain with the best fit for the exponent $\psi$. Given our previous findings for the AG approach indicating that string mass relates to $\tau$ while the cluster mass does not, we would expect a superior fit for the strings. Instead, we find that the exponent $\psi \approx 1.3$ for strings and clusters is identical within the limits of our determination. Essentially, this is a consequence of the fact that the $T$-dependence of $R_g$ is nearly the same for strings and for clusters, while the $T$-dependence of cluster mass differs noticeably. This apparent paradox can be resolved by recognizing that the largest

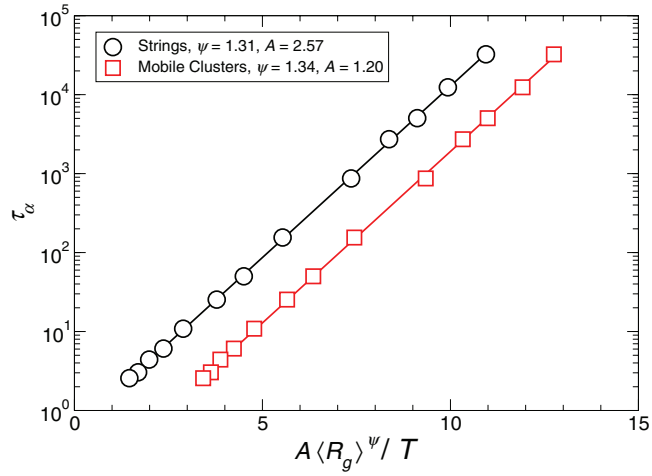


FIG. 17. Testing Eq. (11) to determine the exponent $\psi$ of RFOT. Both the mobile particle clusters and strings yield a consistent fit with $\psi \approx 1.3$. The data for the mobile particle clusters are shifted by two units along the abscissa for clarity of the figure.

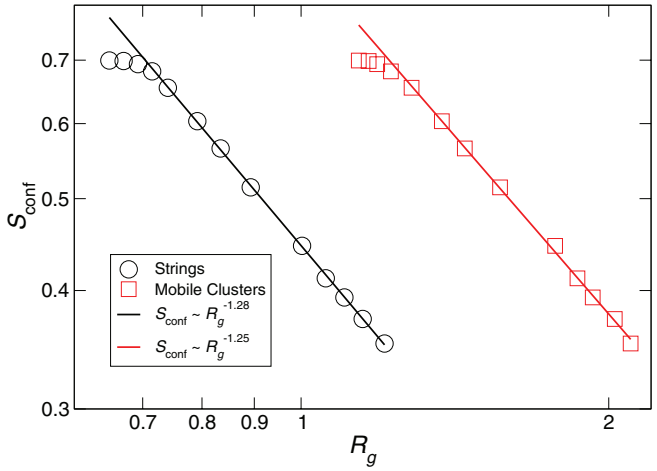


FIG. 18. Evaluation of the surface scaling exponent $\theta$ from the scaling law (Eq. (12)). The value $d_f - \theta \approx 1.3$ is consistent with $\psi$, and with the expectations from AG.

dimension of a cluster dominates $R_g$, so that systems with different mass can have similar $R_g$. This is consistent with the expectation that the largest dimension of mobile clusters is associated with long, string-like clusters.

We next check for consistency of the value $\psi$ with the expectation that $\psi = d_f - \theta$. We can independently determine $d_f - \theta$ from the scaling of $S_{\rm conf}$ with $R_g$ (Eq. (12)), as shown in Fig. 18. While the data deviate from a power-law at high $T$, the lower $T$ data indicate $d_f - \theta \approx 1.3$, consistent with our estimates of $\psi$. The success of these independent approaches significantly increases our confidence in these estimates. Based on our previous findings for $d_f$ for strings, we can also estimate $\theta = 0.3$–$0.7$. The value of $\theta$ is small in comparison with values estimated Refs. 42, 80, and 84. However, a small value for $\theta$ is physically plausible. For example, in the Ising spin glass, a direct evaluation yields $\theta \approx 0.2$–$0.35$ in three dimensions.[83,86,87] Moreover, our value obeys the expected inequality $\theta \leq \psi \leq d - 1$, which the previous estimates violate.[42,80,84]

While both string and mobile particle cluster sizes demonstrate reasonably scaling within RFOT, it appears the success of the cluster description is dependent on the limiting dimension dictated by the string size. The strings also appeared to be the only reasonable description of CRR within the AG framework. Hence, we can find a satisfying consistency for both the AG and RFOT descriptions using the strings as a measure of CRR or mosaic scale, where the exponent values of RFOT are constrained to satisfy the formulation of AG.

## V. DISCUSSION AND CONCLUSION

We have examined the geometrical structure of clusters and string-like cooperative motions in a model glass-forming polymer melt. We found an aesthetically pleasing symmetry in the geometry of high- and low-mobility clusters, i.e., they both conform to statistical geometry of equilibrium branched polymers. In doing so, we also developed a novel method to identify low-mobility particles based on persistent caging. Most importantly, we have examined the question of whether these heterogeneity scales can be identified with the scales anticipated by the AG and RFOT descriptions of glass formation. We found the strings apparently provide the most consistent description of the CRR or mosaic length described by these respective theories.

An important observation arising from our work is that these different quantifications of heterogeneous dynamics in fact correspond to distinct relaxation time scales, and therefore distinct processes of importance in the relaxation of a glass former. In other words, there is no single or unique heterogeneous dynamical scale in the system. These immobile particles are apparently related with the breakdown of the linear scaling between diffusive and viscous relaxation, while the fragility of glass-formation is apparently more related to string-like cooperative motion.[34] Thus, conventional wisdom regarding the role of heterogeneous dynamics on typical aspects of glassy behavior, requires further examination. Apparently, there is no single dynamic heterogeneity scale in glass-forming liquids.

There is further evidence of these scales and their significance on condensed matter relaxation. For example, recent simulations of superheated Ni crystals[82] also find a large increase of the non-Gaussian parameter, mobile particle clusters, and string-like collective motion. However, in this system, there are no immobile particle clusters of finite extent present; there are only immobile atoms in a crystal lattice, and mobile particles having the usual constituent strings. Significantly, there is no decoupling of structural relaxation from the self-intermediate scattering function and the diffusion coefficient, nor any stretched exponential decay of the self-intermediate scattering function in the superheated crystal. Similarly, in a recent study[85,88] on the dependence of dynamics on spatial dimensionality, it is found that the degree of Stokes-Einstein breakdown decreases while the fragility paradoxically increases with spatial dimensionality for dimensionality greater than two. The findings of these studies suggest that the immobile particle clusters, rather than mobile particles, are primarily responsible for decoupling and stretched exponential stress relaxation of glass-forming liquids. This possibility merits systematic study and points to the different types of heterogeneity (mobile and immobile particles) having significantly different impacts on the fluid dynamics. In other words, dynamic heterogeneity comes in different types that must be properly discriminated.

As we alluded to earlier, another common approach to extract a length scale for heterogeneity is via a four-point correlation function. Proper determination of the four-point scale $\xi_4$ can be strongly affected by finite size,[43,91] but careful extractions have show that $\xi_4$ grows more rapidly than would be expected for the CRR of the AG theory.[42] It is possible that $\xi_4$ could be consistent with the mosaic scale of the RFOT theory, but we expect a single measure should be compatible with both approaches, since they are largely complementary. The reason for the difference in the scaling of $\xi_4$ with that observed for the strings can be readily understood by considering their characteristic times; $\xi_4$ is determined at the time of the peak in the four-point susceptibility, which has essentially the same temperature dependence as $\tau_\alpha$. As we have shown, $\tau_\alpha$ is also the time scale of immobile particles, and is distinct

from the time scale (and hence length scale) of mobile particles and strings. Accordingly, $\xi_4$ is primarily sensitive to particles of low mobility.[59] This is a consequence of the fact that, in defining the four-point function, a particle size $a$ is introduced to limit the effects of vibrational motion, and is chosen to be larger than the typical cage size, following Ref. 39. The choice of $a$ controls the scale of relaxation associated with the four-point function. Choosing a smaller value of $a$, closer to the cage size, for example, should lead to a measure of heterogeneity on a smaller time scale, perhaps similar to $t^*$; such a choice would presumably be more sensitive to string-like excitations. Efforts in this direction, along with other approaches to extract the size scale of string-like cooperativity, would be valuable to better understand the findings of the present paper within a more traditional liquid-state correlation function approach.

In conclusion, the analysis of the relationship between the various clusters in the context of the AG and RFOT theories reveals that the strings are a particularly good candidate for the CRR of AG theory. While a similar conclusion may also be reached in the context of RFOT, the fact that all the heterogeneous clusters considered here show fractal structure with a fractal dimension lower than $d = 3$ makes a conclusive comparison difficult at this time, since the mosaic picture in the RFOT framework normally assumes the rearranging regions to be compact. Consequently, it will be valuable to revisit the formulation of RFOT, as the suggested fractal nature of the entropic droplets has implications for the concept of the effective surface tension of these regions.

## ACKNOWLEDGMENTS

J.F.D. acknowledges support from National Institutes of Health (NIH) Grant No. 1 R01 EB006398-01A1. F.W.S. acknowledges support from National Science Foundation (NSF) Grant No. CNS-0959856 and ACS-PRF Grant No. 51983-ND7.

## APPENDIX A: NON-GAUSSIAN AND DIFFUSIVE TIME SCALES

The non-Gaussian parameter $\alpha_2(t)$ is often used to quantify the deviation of particle or segmental displacements from the Gaussian distribution expected for simple fluids. The maximum deviation occurs at a characteristic time $t^*$, and it is well known that $t^*$ is smaller than $\tau_\alpha$, and has a weaker temperature dependence than $\tau_\alpha$. It is then natural to wonder what physical process $t^*$ relates to.

Combining the Stokes-Einstein relation for spheres

$$D = \frac{k_B T}{6\pi \eta R_h}, \tag{A1}$$

where $D$ is the diffusion coefficient, $\eta$ is the fluid viscosity, and $R_h$ is the particle hydrodynamic radius, with Maxwell's relation $\tau = \eta/G_\infty$ (where $G_\infty$ is the high-frequency shear modulus) leads to

$$\frac{D}{T} \propto \frac{1}{\tau}. \tag{A2}$$

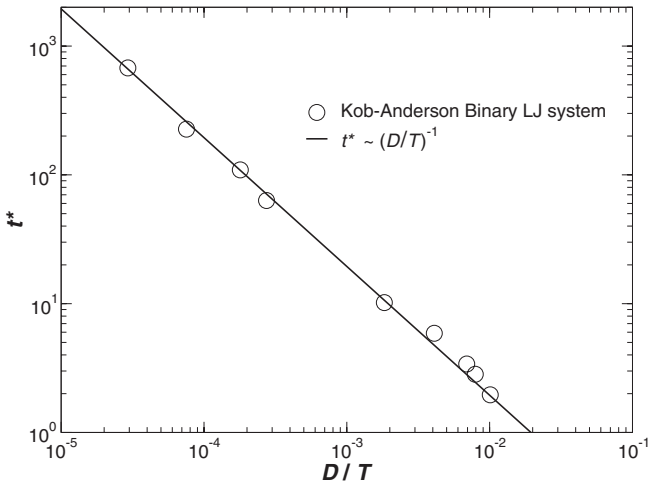


FIG. 19. Linear scaling between $t^*$ and the (inverse) characteristic diffusion time $D/T$ in the Kob-Anderson binary LJ mixture,[49] demonstrating that the time scale $t^*$ corresponds to the time scale for mass diffusion.

In other words, the reduced diffusion coefficient $D/T$ should define an inverse relaxation time. Given the relative slow variation of $t^*$ with $T$ compared to $\tau_\alpha$ from the intermediate scattering function, we check whether $t^*$ can be identified with a diffusive relaxation time defined in this way. Due to the polymeric nature of our system, $D$ cannot be readily evaluated, since mean-squared displacement will only be linear on a much longer time scale, associated with the chain center-of-mass diffusion; this requires chain displacements at least on the order of the chain radius of gyration, more than we can readily simulate at low $T$. However, we can check for a relation between $D/T$ and $t^*$ for the Kob-Anderson binary Lennard-Jones fluid,[49] the most commonly studied computational glass-forming system, where low $T$ data is accessible.

Figure 19 shows that the (inverse) characteristic diffusion time $D/T$ is linear with $t^*$ for the entire range of data, covering several decades. This result clarifies that $t^*$ can be associated with a diffusive time scale. Given the known "decoupling" of structural relaxation and $D/T$ from the Stokes-Einstein relation, we accordingly expect the same decoupling between $t^*$ and $\tau_\alpha$ in our polymer system, as observed in Fig. 1.

It should be appreciated that the decoupling relation between $D$ for the overall chain displacements of a polymer and the long-time shear-stress relaxation time can exhibit a separate relationship from $t^*$ and $\tau_\alpha$.[89] This is a consequence of the fact that heterogeneity at the scale of the chain radius of gyration can differ from heterogeneity at the monomer or segmental scale. Thus, in the polymer system, $t^*$ should be thought of as relating to a local monomer diffusive process, and $\tau_\alpha$ to a segmental structural relaxation time.

## APPENDIX B: IMMOBILE PARTICLE DEFINITION

To study the structure of highly immobile particles, we need to devise a physically sensible algorithm that picks out an appropriate subset of low-mobility particles. Since the caging of particles by their neighbors is one of the hallmarks of glass formation, we utilize the concept of "caged particles." To do so, we must identify the cage size. We can formally do

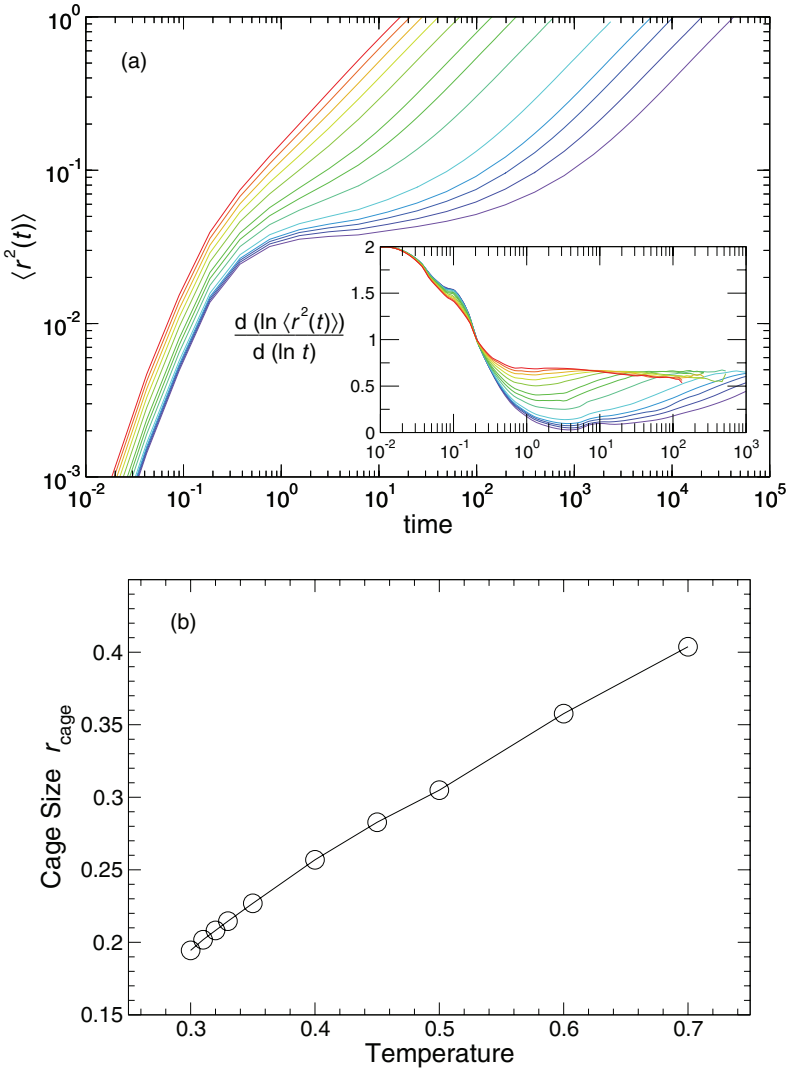


FIG. 20. (a) Identification of the cage size from the mean-squared displacement. The inset shows the logarithmic derivative, which shows a minimum that we use to define $\langle r^2_{cage}\rangle$. (b) The resulting $T$ dependence of the cage size $\langle r^2_{cage}\rangle^{1/2}$. Particles with a squared displacement less than $\langle r^2_{cage}\rangle$ are defined as "caged particles."

this via the mean-squared displacement $\langle r^2(t)\rangle$. Figure 20(a) shows that $\langle r^2(t)\rangle$ has a plateau at a characteristic size in the approximate range 0.04–0.09 (for a cage radius 0.2–0.3). To precisely define the cage size, we take advantage of the fact that the logarithmic derivative $d(\ln\langle r^2(t)\rangle)/d(\ln t)$ exhibits a clear minimum on the time scale of particle caging, $t_{cage}$. We thus define the cage size by $r_{cage} \equiv \langle r^2(t_{cage})\rangle^{1/2}$. We show the $T$ dependence of $r_{cage}$ in Fig. 20(b) for $T \lesssim T_A$; at higher $T$, $\langle r^2(t)\rangle$ transitions from ballistic motion ($d(\ln\langle r^2(t)\rangle)/d(\ln t) = 2$) to sub-diffusive motion ($d(\ln\langle r^2(t)\rangle)/d(\ln t) \approx 0.6$ without intervening particle caging. The sub-diffusive behavior is well known for this model,[46] arising from polymeric effects.

Having unambiguously defined a cage-size, we proceed to track the behavior of caged particles (i.e., particles with displacement less than $r_{cage}$). Figure 21 shows the fraction of caged particles, which, as expected, decreases with time. We note that, formally, this fraction is identical to the "self-overlap" $Q_s(t)$ used in the four-point correlation function formalism,[39] although the particle "size" used is typically fixed at a value 0.3, independent of $T$, and substantially larger than the cage size at low $T$.

Since we wish to understand the tendency for these caged particles to be spatially correlated, we evaluate the average cluster size of these immobile particles. However, we must take into account the fact that the number of these caged particles decreases with time, and thus there is a trivial effect on the cluster size of the number of caged particles. To remove this trivial effect, we normalize the caged particle cluster size by the cluster size of the same fraction of particles chosen at random; this allows us to see how the tendency to cluster compares to the random case, independent of the nature of the underlying dynamics.

Figure 22 shows the normalized cluster size of the caged particles as a function of time. The qualitative behavior matches what we observe for other dynamical clusters: as smaller times, the effect of clustering is weak, and there is a characteristic time where the cluster size reaches a peak. As discussed in the main text, this characteristic time is similar to

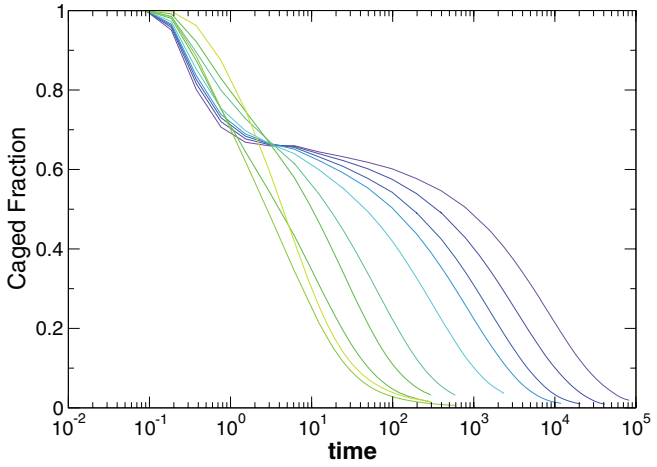


FIG. 21. Dynamical fraction of caged particles for $T < T_A$.

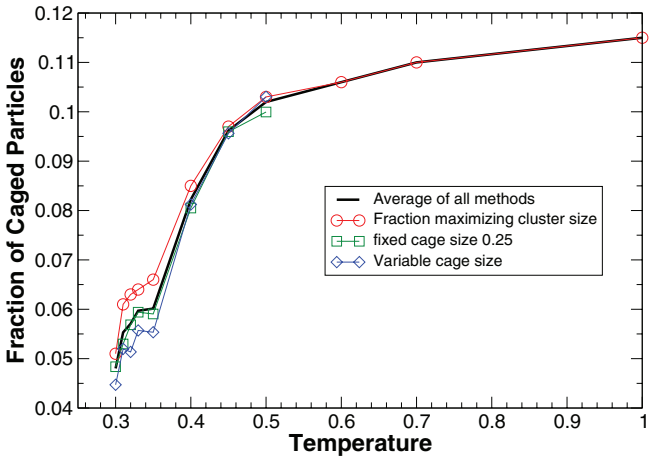


FIG. 23. The characteristic fraction of low mobility particles for several different approaches. All approaches yield similar fractions for all $T$.

the $\alpha$-relaxation time. This time, along with the peak size of the caged-clusters, defines the characteristic features that we wish to capture.

To simplify the analysis of immobile particles and draw a parallel to the analysis of the mobile particles (where there is a fixed, $t$-independent fraction of particles considered), we consider a simplification of this approach that still captures the characteristic peak time and amplitude of caged particles. Specifically, if we look at the characteristic peak time of the caged particles, we can identify the fraction of caged particles at this time, which we show in Fig. 23. This characteristic fraction of caged particles increases with $T$, as the mobility subsets become less distinct at higher $T$. For all subsequent analysis, we use this $T$-dependent fraction for all time, to parallel the approach for the mobile particles. By construction, this fixed fraction reproduces the characteristic time and size the our time-dependent fraction of caged-particles reveals, so that we do not alter these important features.

A natural concern is the sensitivity of this approach to the definition of the cage size, since this is the only parameter that must somehow be chosen. To test this, we also considered a $T$-independent cage size $r_{\text{cage}}$ of 0.2 or 0.25. We find that these $T$ independent sizes of course yield quantitatively different results, but that the time and size scales of the immobile particles all scale in the same way. Additionally, as shown in Fig. 23, the characteristic fraction of caged particles is nearly the same as our definition based on a $T$-dependent cage size, showing the precise definition of cage size does not strongly affect the characteristic immobile fraction.

We also considered another approach to extract the low mobility subset. This approach is motivated by Ref. 52, where they determined a characteristic fraction of highly mobile particles by finding the fraction that maximizes the cluster size formed by those highly mobile particles relative to same fraction of particles chosen at random. This measure provides a way to capture the fraction of particles that most strongly exhibit spatial clustering, without consideration of the underlying mobility distribution. We use the same approach, but finding the fraction of least mobile particles that maximizes the relative clustering. We show this characteristic fraction together with our estimates from the cage size in Fig. 23, and find that we recover nearly the same fraction by this approach. Apparently, the characteristic fraction of immobile particles is not strongly sensitive to the exact choice of parameters, providing confidence in the robustness of our analysis. For the calculations presented in the main body of the manuscript, we simply use the mean of all these estimates.

Finally, we point out that in all approaches to identify low mobility particles, there appears to be an unanticipated feature at $T \approx 0.35$, previously estimated as the characteristic $T_c$ for this system at this density.[48] This is a curious result, but at present we have no explanation for such behavior.

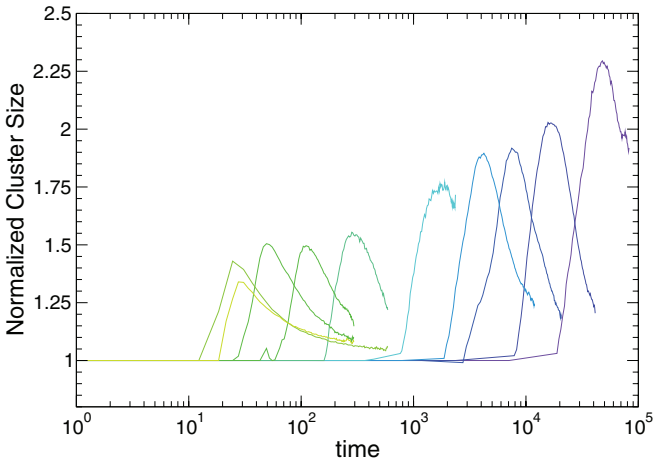


FIG. 22. The normalized cluster size for caged particles for $T < T_A$, where the cage is well-defined.

## APPENDIX C: CALCULATION OF CONFIGURATIONAL ENTROPY

Our goal is the evaluation of the configurational entropy $S_{\text{conf}}$, which enumerates the density of stable potential energy minima sampled by the melt at equilibrium. Procedures for evaluating $S_{\text{conf}}$ have been developed and applied to a variety of systems, including water,[15] binary LJ mixtures,[10,11] silica,[16] and orthoterphenyl.[17] We follow a similar procedure,

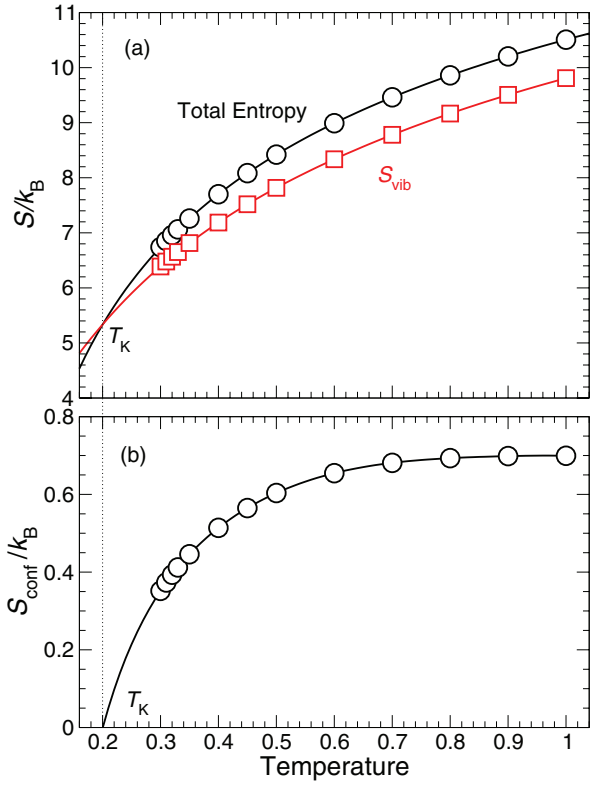


FIG. 24. (a) The total entropy $S$ and vibrational entropy as a function of temperature. (b) The configurational component $S_{conf} = S - S_{vib}$. The line is a guide for the eye.

whereby the overall entropy can be partitioned into vibrational $S_{vib}$ and configurational components, i.e.,

$$S = S_{conf} + S_{vib}. \tag{C1}$$

Our approach will be to evaluate directly $S$ and $S_{vib}$, and by their difference $S_{conf}$ (summarized in Fig. 24).

### 1. Total entropy

To evaluate the absolute entropy of the polymer, we employ the thermodynamic integration technique.[47] In this method, the free energy is calculated by parametrically coupling the potential energy of the system $U_{poly}$ to the potential energy $U_{ref}$ of a reference system for which the free energy can be directly, analytically evaluated. The coupling potential is normally of the form:

$$U(\lambda) = (1-\lambda)U_{polymer} + \lambda U_{ref}, \tag{C2}$$

where the coupling parameter $0 \leq \lambda \leq 1$. The free energy can then be evaluated by

$$F_{poly} = F_{ref} - \int_0^1 \langle U_{ref} - U_{poly}\rangle d\lambda. \tag{C3}$$

This procedure is complicated by the FENE potential that bonds nearest neighbors, since it diverges as the bond length approaches $R_0$. The normally chosen reference potentials do not restrain the bond length, and so the contribution from the FENE potential diverges strongly as $\lambda \to 1$. To avoid this complication, we perform a "two-step" thermodynamic integration, where we first perform an integration from the FENE potential to a harmonic bond potential:

$$U_{harm} = \frac{k_{harm}}{2}(r - R_1)^2 \tag{C4}$$

that does not exhibit the strong divergence as bond length grows; when then perform an integration from the harmonically bonded polymer to the reference system. We choose $k_{harm} = 980$ and $R_1 = 0.87$ so that the location of the minimum and the curvature at the minimum are very near to that of the FENE bond (when combined with the core LJ repulsion). While the free energy for the harmonically bonded polymer is not analytically known, it is not needed, as it drops out in the final expression for the free energy:

$$F_{poly} = F_{ref} - \int_0^1 \langle U_{polymer} - U_{harm}\rangle d\lambda_1 - \int_0^1 \langle U_{ref} - U_{harm}\rangle d\lambda_2. \tag{C5}$$

For the reference potential, we use a potential that shares the system periodicity,[90] namely,

$$U_{ref}(r) = -U_0 \sum_{i=1}^{3} \cos\left(\frac{2\pi}{L} r_i\right), \tag{C6}$$

where $U_0 = 10$ is the amplitude of the potential, $L$ is the length of the container, and $r_i$ is the coordinate of a particle in direction $i$. For an $N$ particle system interacting through $U_{ref}$, evaluation of the partition function shows that

$$F_{ref} = \frac{3N}{\beta} \ln\left(\frac{\rho^{\frac{1}{3}}\Lambda}{I_0(\beta U_0)}\right). \tag{C7}$$

Here $\rho$ is the number density and $I_0$ (x) is the modified Bessel function of the first kind. Combining with Eq. (C5), we have $F$ for the our system at some fixed temperature $T_0$ and density. Accordingly, we can evaluate the entropy for a reference $T_0$,

$$S(T_0) = \frac{E(T_0) - F(T_0)}{T_0}. \tag{C8}$$

We obtain $S$ for any $T$ by exploiting the fact that

$$C_V = T\left(\frac{\partial S}{\partial T}\right)_V = \left(\frac{\partial E}{\partial T}\right)_V, \tag{C9}$$

so that

$$S(T) = \int_{T_0}^{T} \frac{1}{T}\left(\frac{\partial E(T)}{\partial T}\right)_V dT + S(T_0). \tag{C10}$$

The integrand can be evaluated numerically from data for $E(T)$. Since we must explicitly include Planck's constant $\hbar$, we select units appropriate for a monomer of a typical polymer, like polystyrene; specifically, we choose $\epsilon = 1$ kJ/mol, $\sigma = 1$ nm, and $m = 100$ g/mol; using these units, $\hbar = 0.0635078$ kJ ps/mol. The resulting $S(T)$ is shown in Fig. 24(a).

### 2. Vibrational entropy

The vibrational component of the entropy $S_{vib}$ reflects the contributions of the basin shape to the vibrational behavior.

We can partition

$$S_{\rm vib} = S_{\rm harm} + S_{\rm anh}. \tag{C11}$$

In the harmonic approximation, the basin entropy

$$S_{\rm harm} = k_B \sum_{n=1}^{3N-3} \left[ 1 - \ln\left( \frac{\hbar\omega_n}{k_B T} \right) \right], \tag{C12}$$

where $\omega_n$ are the normal modes associated with the basin minimum. To evaluate $\omega_n$, we must first determine the basins associated with the equilibrium liquid. To do so, we perform a conjugate gradient minimization of the potential energy, starting from instantaneous snapshots of the equilibrium polymer; we locate the corresponding minimum, or inherent structure (IS), within a numerical tolerance of $10^{-15}$. Using the configuration at the minimum, we evaluate the Hessian matrix:

$$H_{ij} = \frac{\partial V}{\partial \vec{r}_i \partial \vec{r}_j}, \tag{C13}$$

the matrix of the curvatures of the potential energy. In the harmonic picture, the eigenvalues $\lambda_n = m\omega_n^2$, so we directly obtain the normal modes $\{\omega_n\}$. For each $T$, we generate the IS and $\{\omega_n\}$ for at least 100 configurations that are well-separated temporally.

The anharmonic contribution to $S_{\rm vib}$ for many systems is negligible. To check the anharmonic contribution $S_{\rm anh}$, we first consider an anharmonic energy:

$$E_{\rm anh}(T) = E - \frac{3}{2} N k_B T - e_{\rm IS} \tag{C14}$$

where $e_{\rm IS}$ is the inherent structure energy and $3/2\, Nk_BT$ is the contribution for a harmonic solid. We can then evaluate

$$S_{\rm anh}(T) = \int_0^T \frac{1}{\bar{T}} \frac{\partial E_{\rm anh}}{\partial \bar{T}} d\bar{T}. \tag{C15}$$

To obtain a valid estimate of $E_{\rm anh}$ for a basin, we must heat the IS very rapidly to insure that the system cannot change basins while heating. We perform such heating for at least 100 IS generated from initial equilibrium configurations at $T = 0.31$. In principle, $E_{\rm anh}$ (and thus $S_{\rm anh}$) depend on the equilibrium $T$ from which the ISs are obtained; in practice, we find that the ISs from different $T$ have a nearly identical density of states $\rho(\omega)$ and $E_{\rm anh}(T)$. Hence we can use the behavior of $E_{\rm anh}(T)$ from one set of IS for any $T$. We find that the contribution anharmonic contribution is rather small and negative, and can be well described by $E_{\rm anh} = -0.065\, T$ for $T \leq 0.8$; the results in $S_{\rm anh}(T) = -0.065 \ln T$.

Combining all vibrational contributions, we show $S_{\rm vib}(T)$ in Fig. 24(a), and the resulting $S_{\rm conf}(T) = S(T) - S_{\rm vib}(T)$ in Fig. 24(b).


[1] P. G. Debenedetti and F. H. Stillinger, Nature (London) **410**, 259 (2001).
[2] C. A. Angell, K. L. Ngai, G. B. McKenna, P. F. McMillan, and S. W. Martin, J. Appl. Phys. **88**, 3113 (2000).
[3] M. D. Ediger, Ann. Rev. Phys. Chem. **51**, 99 (2000).
[4] R. Richert, J. Phys.-Condens. Matter **14**, R703 (2002).
[5] C. Donati, S. C. Glotzer, P. H. Poole, W. Kob, and S. J. Plimpton, Phys. Rev. E **60**, 3107 (1999).
[6] G. Adam and J. H. Gibbs, J. Chem. Phys. **43**, 139 (1965).
[7] R. J. Greet and D. Turnbull, J. Chem. Phys. **47**, 2185 (1967).
[8] R. Richert and C. A. Angell, J. Chem. Phys. **108**, 9016 (1998).
[9] C. M. Roland, S. Capaccioli, M. Lucchesi, and R. Casalini, J. Chem. Phys. **120**, 10640 (2004).
[10] F. Sciortino, W. Kob, and P. Tartaglia, Phys. Rev. Lett. **83**, 3214 (1999).
[11] S. Sastry, Nature (London) **409**, 164 (2001).
[12] R. J. Speedy, J. Chem. Phys. **110**, 4559 (1999).
[13] R. J. Speedy, J. Chem. Phys. **114**, 9069 (2001).
[14] L. Angelani and G. Foffi, J. Phys.: Condens. Matter **19**, 256207 (2007).
[15] F. W. Starr, S. Sastry, E. La Nave, A. Scala, H. E. Stanley, and F. Sciortino, Phys. Rev. E **63**, 041201 (2001).
[16] I. Saika-Voivod, F. Sciortino, and P. H. Poole, Phys. Rev. E **69**, 041503 (2004).
[17] S. Mossa, E. La Nave, H. E. Stanley, C. Donati, F. Sciortino, and P. Tartaglia, Phys. Rev. E **65**, 041205 (2002).
[18] T. R. Kirkpatrick, D. Thirumalai, and P. G. Wolynes, Phys. Rev. A **40**, 1045 (1989).
[19] V. Lubchenko and P. G. Wolynes, Ann. Rev. Phys. Chem. **58**, 235 (2007).
[20] J.-P. Bouchaud and G. Biroli, J. Chem. Phys. **121**, 7347 (2004).
[21] C. Donati, J. F. Douglas, W. Kob, S. J. Plimpton, P. H. Poole, and S. C. Glotzer, Phys. Rev. Lett. **80**, 2338 (1998).
[22] M. Aichele, Y. Gebremichael, F. W. Starr, J. Baschnagel, and S. C. Glotzer, J. Chem. Phys. **119**, 5290 (2003).
[23] Y. Gebremichael, M. Vogel, and S. Glotzer, J. Chem. Phys. **120**, 4415 (2004).
[24] R. A. Riggleman, K. Yoshimoto, J. F. Douglas, and J. J. de Pablo, Phys. Rev. Lett. **97**, 045502 (2006).
[25] M. Vogel, B. Doliwa, A. Heuer, and S. Glotzer, J. Chem. Phys. **120**, 4404 (2004).
[26] T. Schroder, S. Sastry, J. Dyre, and S. Glotzer, J. Chem. Phys. **112**, 9834 (2000).
[27] N. Giovambattista, F. W. Starr, F. Sciortino, S. V. Buldyrev, and H. E. Stanley, Phys. Rev. E **65**, 041502 (2002).
[28] A. H. Marcus, J. Schofield, and S. A. Rice, Phys. Rev. E **60**, 5725 (1999).
[29] Z. Zheng, F. Wang, and Y. Han, Phys. Rev. Lett. **107**, 065702 (2011).
[30] Z. Zhang, P. J. Yunker, P. Habdas, and A. G. Yodh, Phys. Rev. Lett. **107**, 208303 (2011).
[31] E. R. Weeks, J. C. Crocker, A. C. Levitt, A. Schofield, and D. A. Weitz, Science **287**, 627 (2000).
[32] N. Giovambattista, S. V. Buldyrev, F. W. Starr, and H. E. Stanley, Phys. Rev. Lett. **90**, 085506 (2003).
[33] Y. Gebremichael, M. Vogel, M. N. J. Bergroth, F. W. Starr, and S. C. Glotzer, J. Phys. Chem. B **109**, 15068 (2005).
[34] F. W. Starr and J. F. Douglas, Phys. Rev. Lett. **106**, 115702 (2011).
[35] B. A. Pazmiño, J. F. Douglas, and F. W. Starr, Soft Matter **9**, 241 (2013).
[36] T. R. Kirkpatrick and D. Thirumalai, Phys. Rev. A **37**, 4439 (1988).
[37] C. Dasgupta, A. V. Indrani, S. Ramaswamy, and M. K. Phani, Europhys. Lett. **15**, 307 (1991).
[38] S. Franz, C. Donati, G. Parisi, and S. C. Glotzer, Philos. Mag. B **79**, 1827 (1999).
[39] N. Lačević, F. W. Starr, T. B. Schrøder, and S. C. Glotzer, J. Chem. Phys. **119**, 7372 (2003).
[40] L. Berthier, G. Biroli, J.-P. Bouchaud, L. Cipelletti, D. E. Masri, D. L'Hôte, F. Ladieu, and M. Pierno, Science **310**, 1797 (2005).
[41] G. Biroli, J.-P. Bouchaud, K. Miyazaki, and D. R. Reichman, Phys. Rev. Lett. **97**, 195701 (2006).
[42] S. Karmakar, C. Dasgupta, and S. Sastry, Proc. Natl. Acad. Sci. U.S.A. **106**, 3675 (2009).
[43] S. Karmakar, C. Dasgupta, and S. Sastry, Phys. Rev. Lett. **105**, 015701 (2010).
[44] E. Flenner and G. Szamel, Phys. Rev. Lett. **105**, 217801 (2010).
[45] G. S. Grest and K. Kremer, Phys. Rev. A **33**, 3628 (1986).
[46] J.-L. Barrat, J. Baschnagel, and A. Lyulin, Soft Matter **6**, 3430 (2010).
[47] D. Frenkel and B. Smit, *Understanding Molecular Simulation From Algorithms to Applications* (Academic, San Diego, CA, 1996).
[48] F. W. Starr, S. Sastry, J. F. Douglas, and S. C. Glotzer, Phys. Rev. Lett. **89**, 125501 (2002).
[49] W. Kob and H. C. Andersen, Phys. Rev. E **51**, 4626 (1995).
[50] F. Sciortino, P. Gallo, P. Tartaglia, and S.-H. Chen, Phys. Rev. E **54**, 6331 (1996).
[51] W. Kob, C. Donati, S. J. Plimpton, P. H. Poole, and S. C. Glotzer, Phys. Rev. Lett. **79**, 2827 (1997).
[52] Y. Gebremichael, T. B. Schrøder, F. W. Starr, and S. C. Glotzer, Phys. Rev. E **64**, 051503 (2001).
[53] D. Thirumalai and R. D. Mountain, Phys. Rev. E **47**, 479 (1993).
[54] K. Vollmayr-Lee and A. Zippelius, Phys. Rev. E **72**, 041507 (2005).

[55]K. Vollmayr-Lee, W. Kob, K. Binder, and A. Zippelius, J. Chem. Phys. **116**, 5158 (2002).
[56]M. Dzugutov, S. I. Simdyankin, and F. H. M. Zetterling, Phys. Rev. Lett. **89**, 195701 (2002).
[57]H. Tanaka, J. Non-Cryst. Solids **351**, 3385 (2005).
[58]H. Tanaka, T. Kawasaki, H. Shintani, and K. Watanabe, Nat. Mater. **9**, 324 (2010).
[59]J. C. Conrad, P. P. Dhillon, E. R. Weeks, D. R. Reichman, and D. A. Weitz, Phys. Rev. Lett. **97**, 265701 (2006).
[60]A. V. Anikeenko and N. N. Medvedev, Phys. Rev. Lett. **98**, 235504 (2007).
[61]U. R. Pedersen, T. B. Schrøder, J. C. Dyre, and P. Harrowell, Phys. Rev. Lett. **104**, 105701 (2010).
[62]D. Stauffer and A. Aharony, *Introduction To Percolation Theory* (Taylor and Francis, London, 1998).
[63]D. S. Gaunt, M. F. Sykes, G. M. Torrie, and S. G. Whittington, J. Phys. A **15**, 3209 (1982).
[64]E. J. J. van Rensburg and N. Madras, J. Phys. A **30**, 8035 (1997).
[65]H.-K. Janssen and O. Stenull, Phys. Rev. E **85**, 051126 (2012).
[66]N. Jan and D. Stauffer, Int. J. Mod. Phys. C **09**, 341 (1998).
[67]N. Giovambattista, S. V. Buldyrev, F. W. Starr, and H. E. Stanley, Phys. Rev. E **72**, 011202 (2005).
[68]H. E. Castillo, C. Chamon, L. F. Cugliandolo, J. L. Iguain, and M. P. Kennett, Phys. Rev. B **68**, 134442 (2003).
[69]J. F. Douglas, Phys. Rev. E **54**, 2677 (1996).
[70]J.-S. Wang and D. Stauffer, Z. Phys. B: Condens. Matter **78**, 145 (1990).
[71]G. Paul, R. M. Ziff, and H. E. Stanley, Phys. Rev. E **64**, 026115 (2001).
[72]F. Family, T. Vicsek, and P. Meakin, Phys. Rev. Lett. **55**, 641 (1985).
[73]J. F. Douglas, J. Dudowicz, and K. F. Freed, J. Chem. Phys. **125**, 144907 (2006).
[74]K. F. Freed, *Renormalization Group Theory of Macromolecules* (Wiley-Interscience, New York, 1987).
[75]J. P. Wittmer, A. Milchev, and M. E. Cates, J. Chem. Phys. **109**, 834 (1998).
[76]J. D. Stevenson, J. Schmalian, and P. G. Wolynes, Nat. Phys. **2**, 268 (2006).
[77]J. F. Kincaid, H. Eyring, and A. E. Stearn, Chem. Rev. **28**, 301 (1941).
[78]R. M. Barrer, Trans. Faraday Soc. **39**, 48 (1943).
[79]L. Qun-Fang, H. Yu-Chun, and L. Rui-Sen, Fluid Phase Equilib. **140**, 221 (1997).
[80]C. Cammarota, A. Cavagna, G. Gradenigo, T. S. Grigera, and P. Verrocchio, J. Chem. Phys. **131**, 194901 (2009).
[81]T. Das, S. Sengupta, and M. Rao, Phys. Rev. E **82**, 041115 (2010).
[82]H. Zhang, M. Khalkhali, Q. Liu, and J. F. Douglas, J. Chem. Phys. **138**, 12A538 (2013).
[83]D. S. Fisher and D. A. Huse, Phys. Rev. B **38**, 386 (1988).
[84]S. Capaccioli, G. Ruocco, and F. Zamponi, J. Phys. Chem. B **112**, 10652 (2008).
[85]S. Sengupta, S. Karmakar, C. Dasgupta, and S. Sastry, Phys. Rev. Lett. **109**, 095705 (2012).
[86]W. L. McMillan, Phys. Rev. B **30**, 476 (1984).
[87]A. J. Bray and M. A. Moore, J. Phys. C: Solid State Phys. **17**, L463 (1984).
[88]S. Sengupta, S. Karmakar, C. Dasgupta, and S. Sastry, "Breakdown of the Stokes-Einstein relation in two, three, and four dimensions," J. Chem. Phys. (this special topic issue).
[89]A. P. Sokolov and K. S. Schweizer, Phys. Rev. Lett. **102**, 248301 (2009).
[90]F. Vargas Lara and F. W. Starr, Soft Matter **7**, 2085 (2011).
[91]S. Karmakar and I. Procaccia, Phys. Rev. E **86**, 061502 (2012).